Electronic Supplementary Material (ESI) for Physical Chemistry Chemical Physics.

Supporting Information for

A Bottom-up approach to the ion recognition mechanism of K+ channels from the laser spectroscopy of hydrated partial peptide - alkali metal ion complexes

Yukina Suzuki[1,2], Keisuke Hirata[1,3,4], James M. Lisy[4,5*], Shun-ichi Ishiuchi[1,3,4*] and Masaaki Fujii[1,2,4*]

[1]*Laboratory for Chemistry and Life Science, Institute of Innovative Research, Tokyo Institute of Technology. 4259 Nagatsuta-cho, Midori-ku, Yokohama, 226-8503, Japan.*

[2]*School of Life Science and Technology, Tokyo Institute of Technology. 4259 Nagatsuta-cho, Midori-ku, Yokohama, Kanagawa, 226-8503, Japan.*

[3]*Department of Chemistry, School of Science, Tokyo Institute of Technology, 2-12-1 Ookayama, Meguro-ku, Tokyo 152-8550, Japan.*

[4]*Tokyo Tech World Research Hub Initiative (WRHI), Institute of Innovation Research, Tokyo Institute of Technology, 4259, Nagatsuta-cho, Midori-ku, Yokohama, 226-8503, Japan.*

[5]*Department of Chemistry, University of Illinois at Urbana-Champaign, Urbana, IL 61801, USA.*

[*] Corresponding authors

JML: j-lisy@illinois.edu, SI: ishiuchi.s.aa@m.titech.ac.jp, MF: mfujii@res.titech.ac.jp

Experimental setup

Fig. S 1 shows the experimental setup used in this study[1]. The ions continuously sprayed from the ESI source are trapped for 100 ms in the LIT at selected temperatures (80 K-300 K).

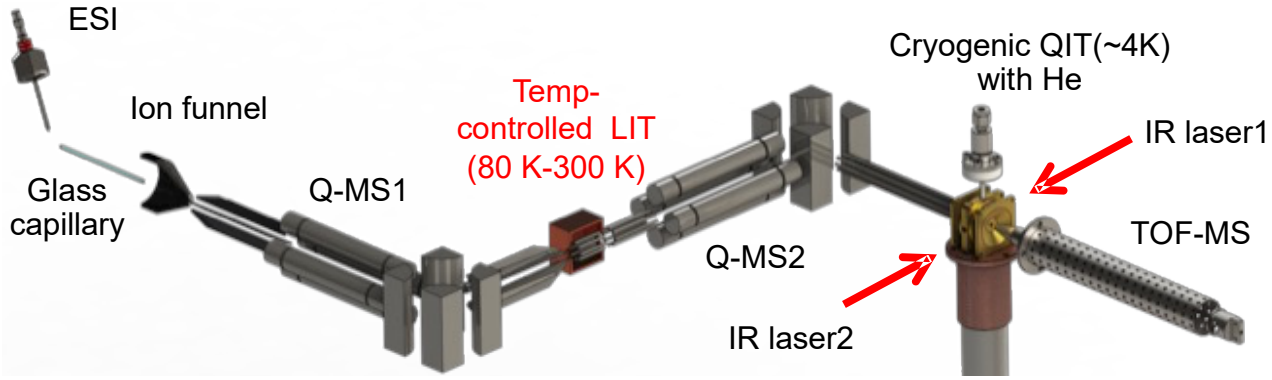

Fig. S 1 Experimental setup. The temperature-controlled linear ion trap (LIT) is denoted in red.

Timing of 2-color IRPD

Fig. S 2 shows a schematic diagram of delays for each component of the experimental setup for the 2-color IRPD measurement. The experiment was operated in the 10 Hz cycle. The ions of the selected mass from the ESI source were collected into the LIT and trapped for 100 ms. The gas of H_2O vapor and He was injected at t=85 ms (about 85 ms after the trapping of ions in the LIT). The first laser (IR1) operating at 5Hz irradiated the ions in the QIT ~50 ns prior to the second laser (IR2). Fig. S 3 is a schematic diagram for 2-color IRPD measurement.

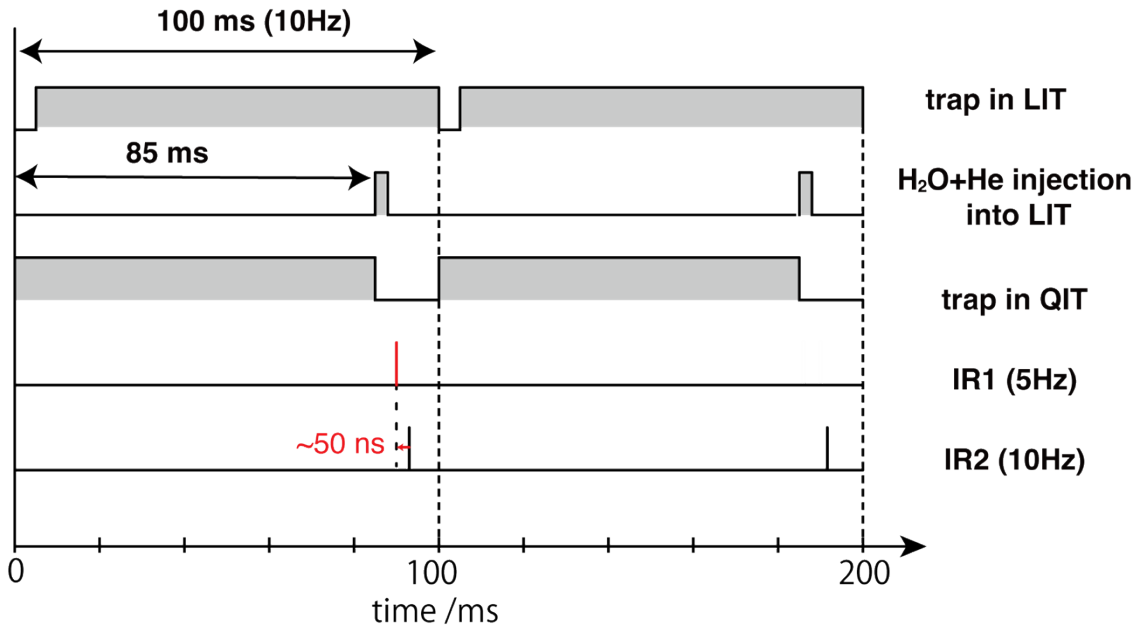

Fig. S 2 The timing of each component of the experimental setup for measuring 2-color IRPD spectra.

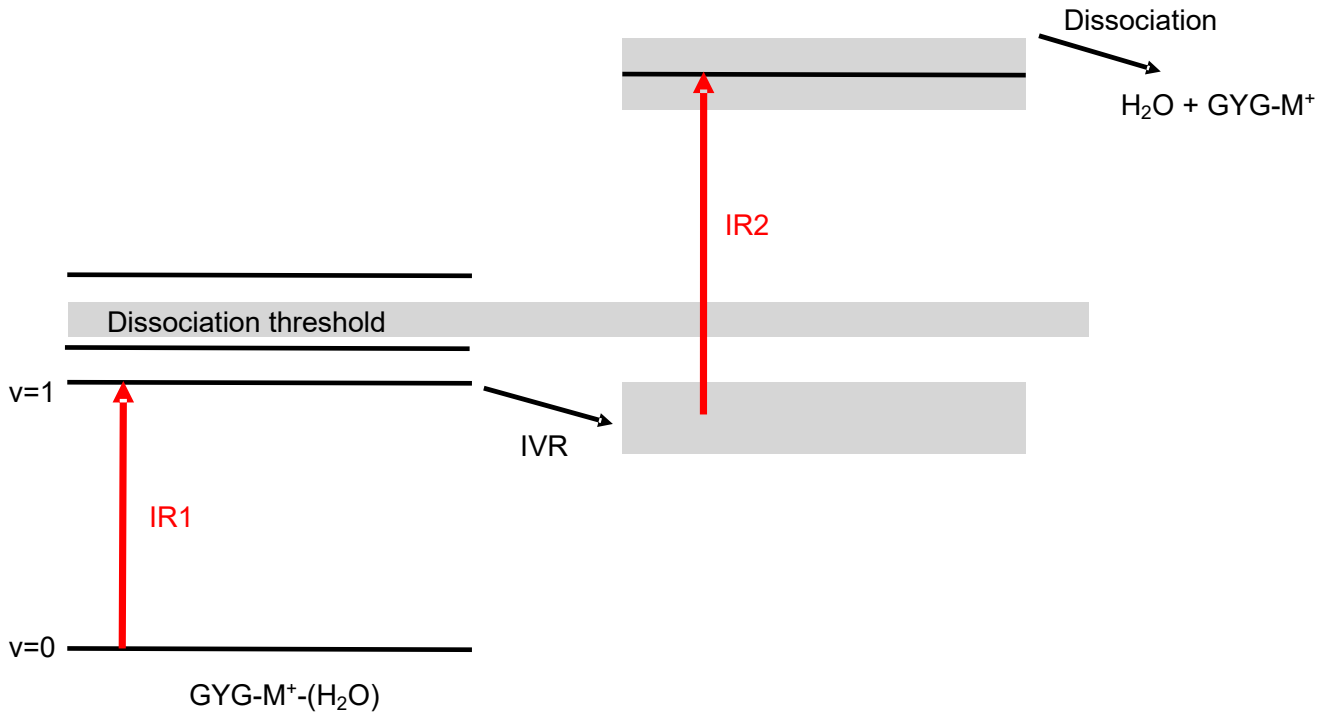

Fig. S 3 A schematic diagram of the 2-color IRPD scheme. IR1 excites the ions from the ground to a vibrationally excited state. The energy is then distributed via the intramolecular vibrational energy redistribution. The ions in the dense states absorb a photon from IR2 and dissociate into H_2O and GYG-M^+.

Single-IRPD and 2-color IRPD

Fig. S 4 and Fig. S 5 compare the spectra of GYG-Li/K^+-H_2O measured by monitoring the dissociated

fragments, GYG-Li/K^+, via either a single IRPD (red) or 2-color IRPD (blue). IR2 for the 2-color IRPD measurement was fixed at 3637cm^{-1} and 3630 cm^{-1}, respectively, for Li^+ and K^+. The intensities of NH stretches are significantly reduced in the single IRPD spectrum. This indicates that the binding energy of the water in GYG-Li^+-H_2O is close to the photon energy in the NH stretch region. We employed the 2-color IRPD method to enhance the IRPD signal. A comparison of the single IRPD spectra and 2-color IRPD spectra of the K^+ complex in Fig. S 5 shows a relatively small change in the NH stretches patterns, and thus the 2-color IRPD methods does not significantly alter the observed conformer population.

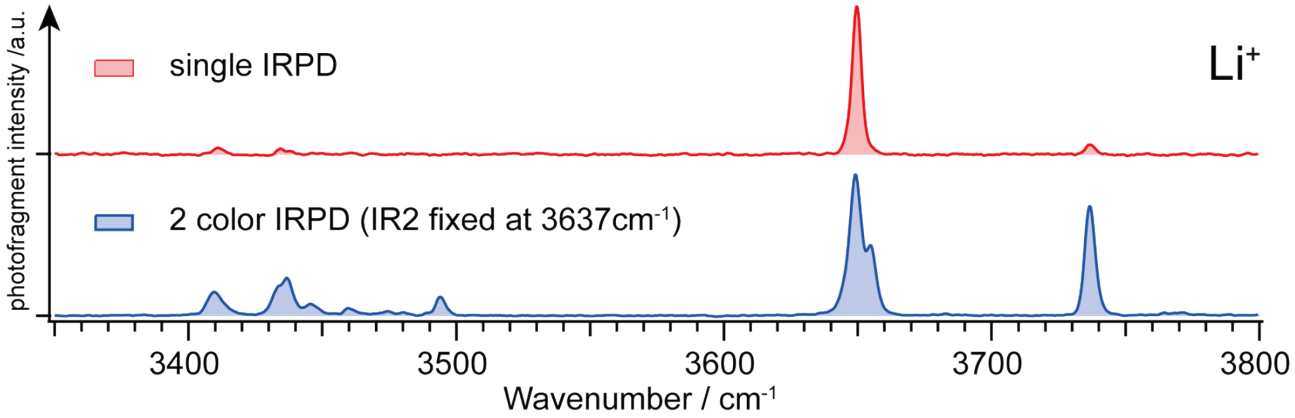

Fig. S 4 The single IRPD and 2-color IRPD (IR2 fixed at 3637cm^{-1}) spectra of the hydrated Li^+ complex. The intensity of NH stretches in the single IRPD spectrum is significantly reduced compared to those in the 2-color IRPD spectrum.

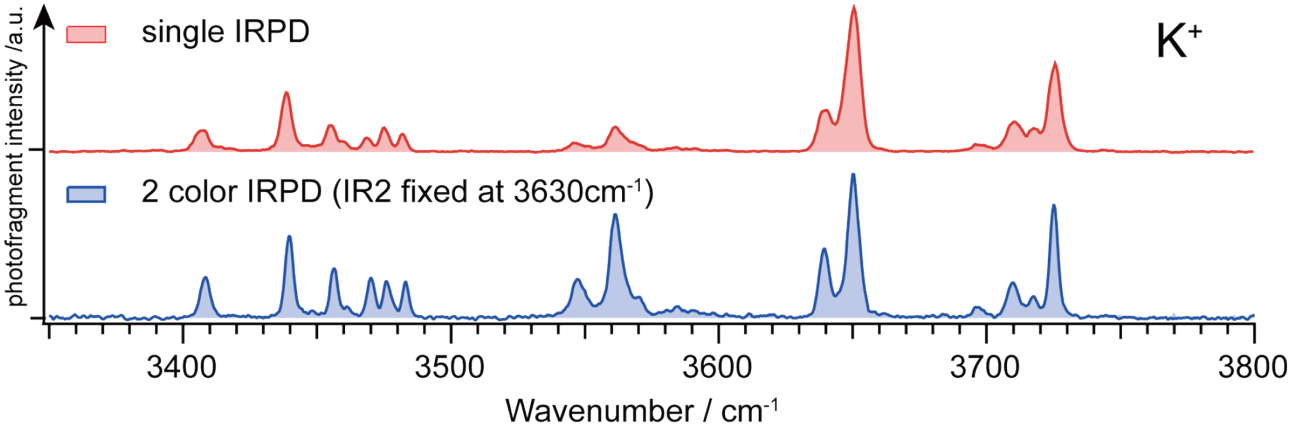

Fig. S 5 The single IRPD and 2-color IRPD with IR2 fixed at 3630 cm^{-1} spectra of the hydrated K^+ complex. The two spectra give similar patterns in the NH stretch region.

2-color IRPD frequency dependence

Fig. S 6 shows the "hot bands" (photodissociation spectra of the vibrationally excited ions by the first laser) on the left panel and 2-color IRPD spectra of Li^+, Na^+, and K^+ complexes on the right. The hot bands were measured by fixing the first IR laser (5 Hz) at a frequency associated with a characteristic band of a specific conformer while scanning the other IR2 laser (10 Hz). For this experiment, in contrast to the 2-color IRPD explained in the main text, the fixed laser and scanned laser were reversed. IR1 excites a specific conformer ~50 ns before IR2 irradiates the entire cluster ion ensemble (including the conformer excited by IR1). IR2 is scanned to probe the photodissociation of the entire ensemble including the vibrationally excited ions from the IR1 excitation. The red spectra were measured with only IR2 and correspond to the typical single IRPD spectra. The black spectra were measured with both lasers on and show the "hot bands" induced by the excitation from IR1 and are observed as broad shoulders for each conformer, though the intensities vary depending on the conformer. The blue lines in the hot band spectra indicate the selected frequency for 2-color IRPD measurement on the right panel. The 2-color IRPD spectra, measured by fixing IR2, at these frequencies are shown on the right. For Li^+ and Na^+, which show only negligible/slight temperature dependence of the spectra, the NH stretches are almost the same regardless of the IR2 frequency. For the K^+ complex, which displays the most significant temperature dependence, intensities of the O/O/R conformer change slightly. Although the change is larger than the Li^+ and Na^+ complexes, we used the same frequency throughout the temperature-dependence experiment. Since our focus is on the relative change and trend of the population with changing the temperature, the slight dependence of the IR2 frequency does not affect our discussion.

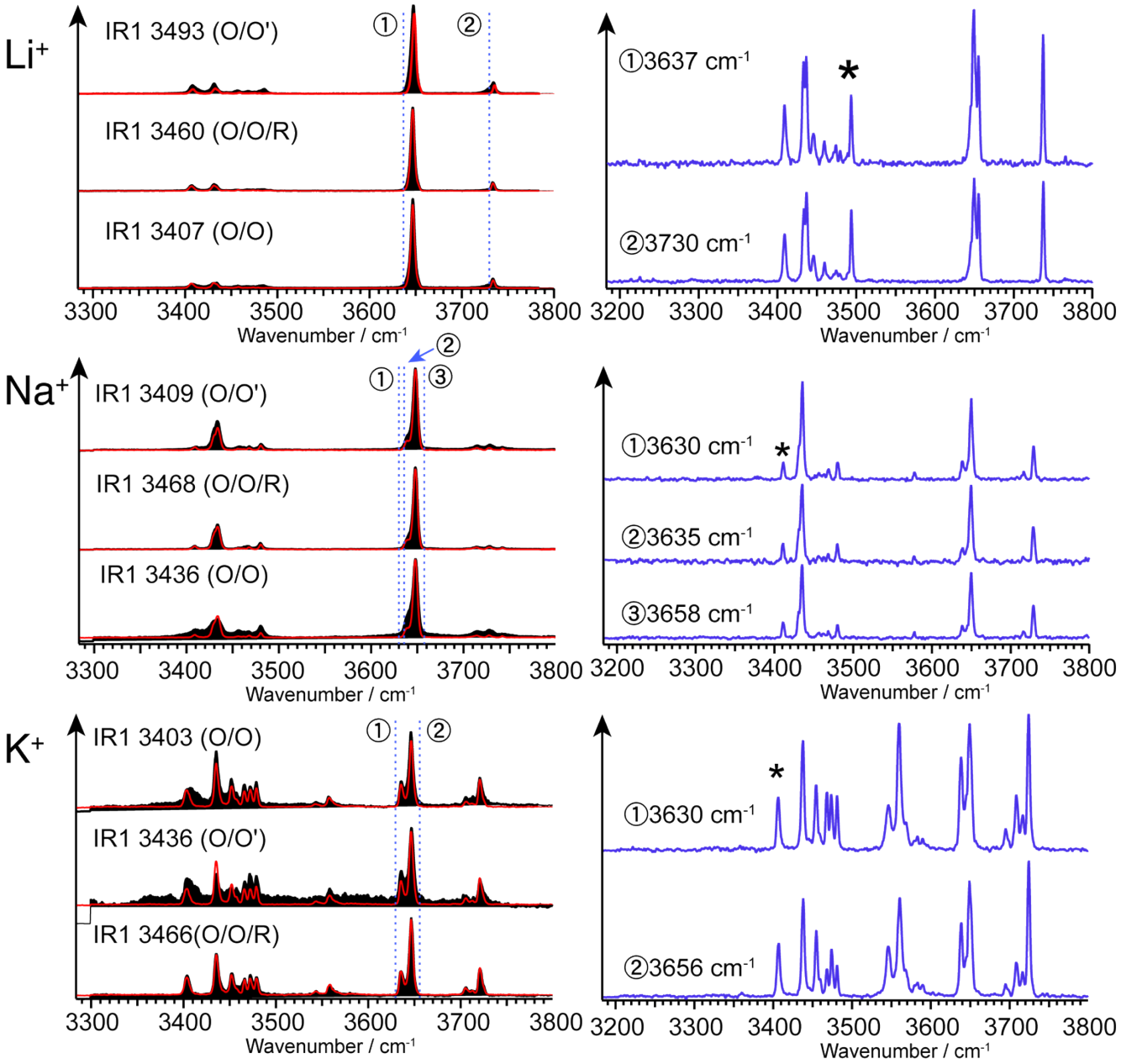

Fig. S 6 Frequency dependence of the fixed IR laser for the hydrated Li, Na, and K complexes. The left panels show the fixed frequencies for laser (IR1 – 5 Hz) corresponding to the indicated conformer. Numbers 1 and 2 are the frequencies for the fixed frequencies for the two color IRPD spectra (IR2 - 10 Hz) shown in the right panels. The spectra are normalized to the band marked with *, respectively.

IR-UV dip (conformer selective spectra)

As stated in the main text, multiple conformers coexist in the spectra, and conformer-specific spectra are helpful for the detailed structural assignment of each conformer. To separate the spectra by conformer, we measured IR-UV spectra for Li^+, Na^+, Rb^+ and Cs^+, and IR-IR spectra for Na^+ and Rb^+ (Fig. S 8, Fig. S 9, Fig. S 10, and Fig. S 11). The conformer-selective spectra were measured at 180 K with the exception of the O/O/R conformer of Na^+. The LIT was cooled down to 150 K to increase the ion intensity of this relatively weak Na^+ O/O/R. The 2-color IRPD displayed in Fig. S 8 – Fig. S 11 on the bottom of the figures are the spectra at 180 K. These obtained spectra are assigned with the assistance of theoretical spectra from DFT calculations. The conformational search was carried out with the following strategy based on the previous study[2]. Specifically, one water molecule was added to the three peptide conformations, O/O, O/O', and O/O/R, observed in the non-hydrated GYG-M^+ complex, to the following possible water binding sites: 1). Metal ion, 2). Carbonyl oxygens, 3). NH groups, 4). Benzene ring 5). TyrOH (Fig. S 7). These water configurations were calculated for each peptide conformer, O/O, O/O', and O/O/R.

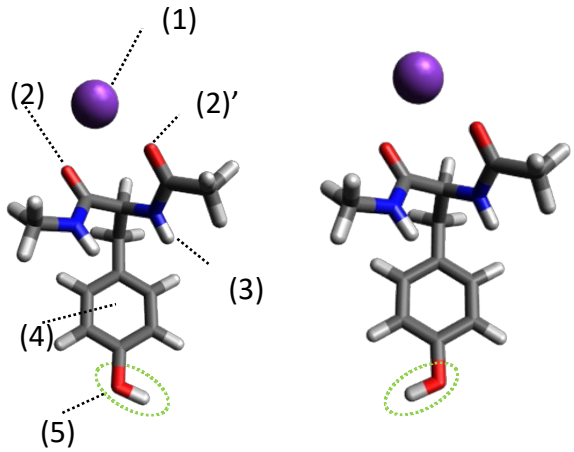

Fig. S 7 Water binding sites. (1) metal, (2), (2)' carbonyl (3) NH (4) benzene (π) (5) TyrOH, as shown using the O/O conformer as an example. TyrOH (circled in green) rotamers exist for each conformer.

Li^+ complex

For GYG-Li^+-H_2O, the three IR-UV dip spectra are displayed in Fig. S 8 with the calculated harmonic frequencies of assigned structures and the IRPD spectra at 180 K. By comparing the patterns of NH stretches of the non-hydrated species and mono-hydrated ones, we can characterize the peptide structure for each spectrum, in this case, O/O/R, O/O', and O/O from the top. From the previous studies[3, 4], the O/O/R conformer has relatively a small splitting in two NH stretches since both Hs in the NH groups are facing away and free from interactions with the benzene ring, and is well described by the blue spectrum on the top. The O/O' conformer, on the other hand, has a larger splitting due to one NH group (AceME) interacting with the phenyl ring, while the other NH group (NHMe), does not. The red spectrum, therefore, is assigned to O/O' due to the largest splitting. The O/O conformer has both NH groups interacting with the benzene ring and is characterized by a smaller splitting to lower frequency, which captures the features of the green spectrum. For water interactions, all the spectra show free water OH stretches, the symmetric stretch around 3650 cm^{-1}, and the asymmetric stretch around 3737 cm^{-1}. Therefore, the structures corresponding to these spectra have the water molecule interacting only with the metal ion (1. metal). The spectra of these peptide structures (O/O, O/O', and O/O/R) of the metal configurations are shown in the figure and agree well with the experimental spectra. The calculated spectra of structures with other water-binding sites are shown in Fig. S 12 – Fig. S 14.

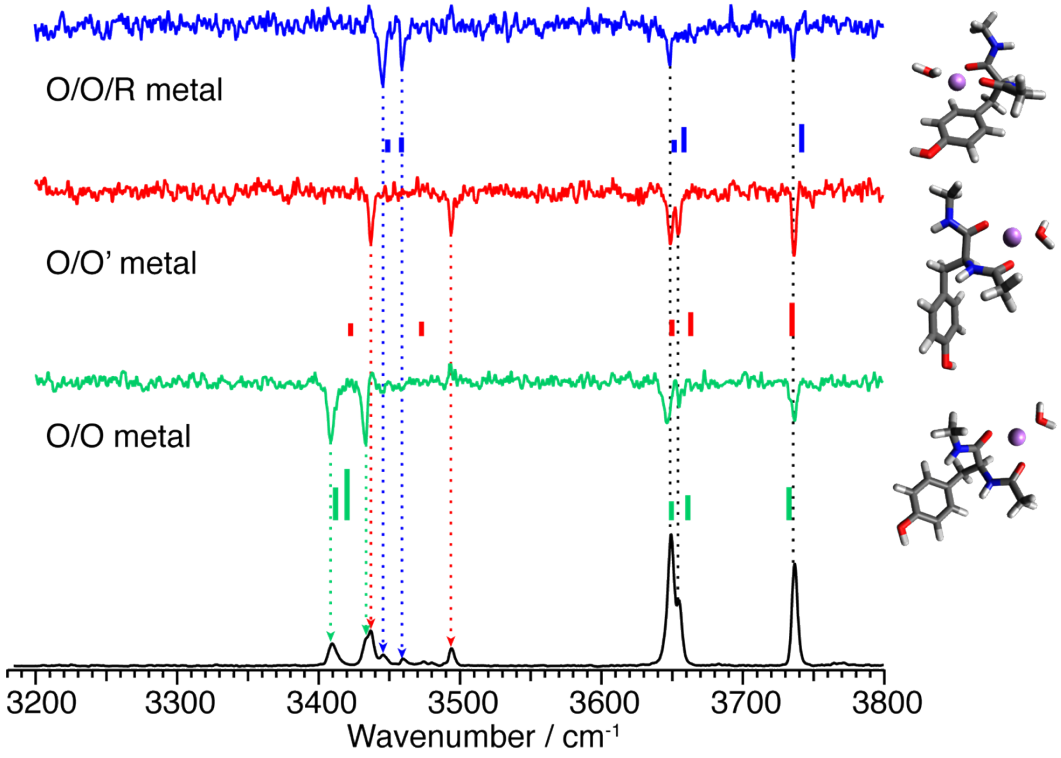

Fig. S 8 The IR-UV dip spectra of the hydrated Li^+ complex with the 2-color IRPD spectrum at the bottom. The calculated spectrum and structure for each conformer are shown below/beside the experimental spectrum.

Na^+ complex

IR-UV dip spectra were not reported in the previous study[2] for GYG-Na^+-H_2O, but have been measured and reported for this study. The figure shows the IR-UV dip spectra and calculated theoretical IR spectra and their structures. As the IR-UV spectrum of the O/O/R conformer was weak due to the small fragmentation intensities, we measured the spectrum of O/O/R by IR-IR dip spectroscopy. The overall IRPD spectrum of GYG-Na^+-H_2O shows negligible hydrogen bonding (similar to GYG-Li^+-H_2O). This is due to the small (~15%) contribution of the O/O/R conformer to the cluster ion ensemble at 180 K. However, it is quite clear from the IR-IR spectrum that there is a hydrogen bond between one OH group on water and the oxygen lone pair of the tyrosine OH group.

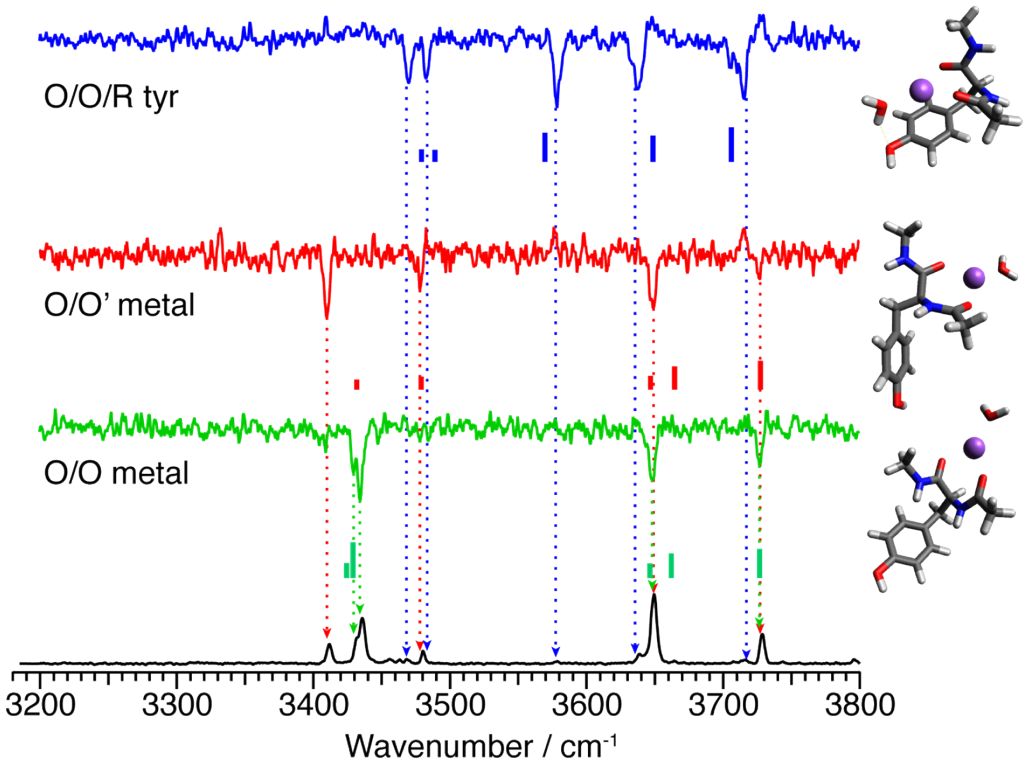

Fig. S 9 The IR-UV (for O/O and O/O') and IR-IR (for O/O/R) dip spectra of the hydrated Na^+ complex with the 2-color IRPD spectrum at the bottom. The calculated spectrum and structure for each conformer are shown below/beside the experimental spectrum.

Rb and Cs^+ complex

For GYG-Rb^+-H_2O and GYG-Cs^+-H_2O (Fig. S 10 and Fig. S 11 respectively), four spectra, similar to GYG-K^+-H_2O were obtained, the first three with H-bonded OH stretches in the 3500-3550 cm^{-1} region and the fourth one with a red-shifted H-bonded OH stretch around 3450 cm^{-1}. The spectrum of this last GYG-Rb^+-H_2O conformer was also measured by IR-IR dip spectroscopy to enhanced peaks that were weakly observed in the IR-UV spectrum. The first three spectra, again, show similar features of previously observed conformers, O/O, O/O', and O/O/R, and are compared with the calculated spectra of these conformers with different water binding sites. For the three spectra, the calculated spectrum of each reported peptide conformation, with water H-bonding to a carbonyl oxygen for O/O and O/O' and the tyrosine OH for O/O/R, shows good agreement with the observed spectra. However, none of the structures of the above peptide conformations and water-binding sites reproduced the fourth spectrum. Therefore, a further conformational search was conducted, and will be discussed below. The fourth spectrum for both ions was assigned to a new peptide conformation, O/R, as shown beside the spectrum. In this conformation, the metal is directly binding to the peptide through one of the carbonyl oxygens and the π cloud of the benzene ring. The water inserts between the other carbonyl oxygen and the metal ion, forming a hydrogen bond. The calculated spectra of structures with other water-binding sites for GYG-Rb^+-H_2O are shown in Fig. S 15 – Fig. S 17, and for GYG-Cs^+-H_2O in Fig. S 18 – Fig. S 20.

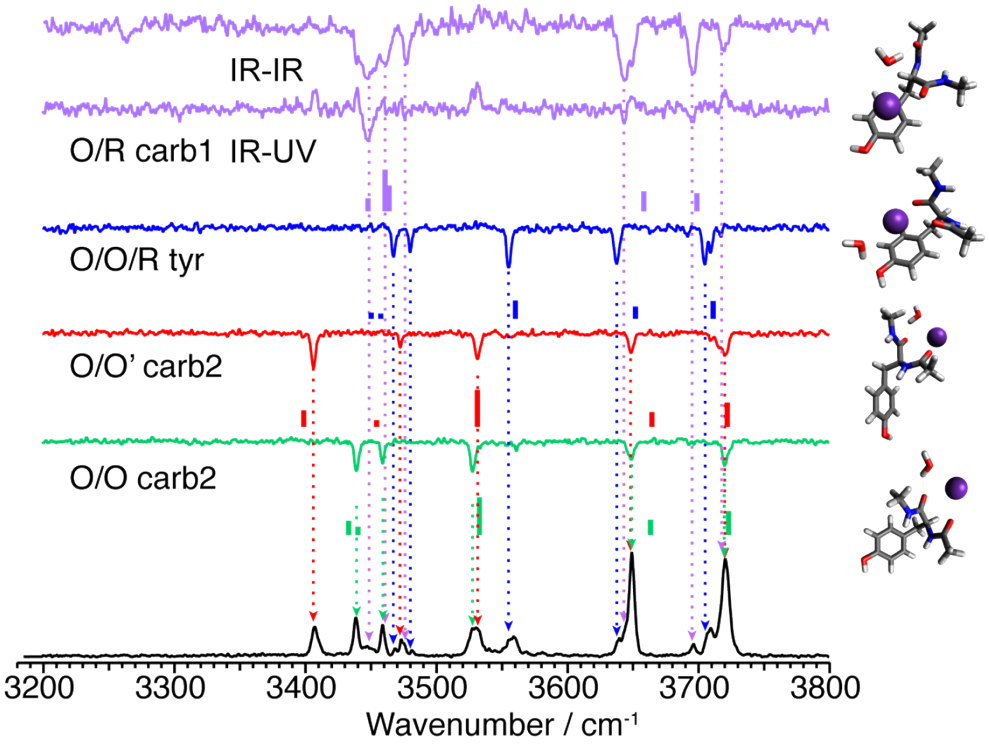

Fig. S 10 The IR-UV and IR-IR (for O/R) dip spectra of the hydrated Rb^+ complex with the 2-color IRPD spectrum at the bottom. The calculated spectrum and structure for each conformer are shown below/beside the experimental spectrum.

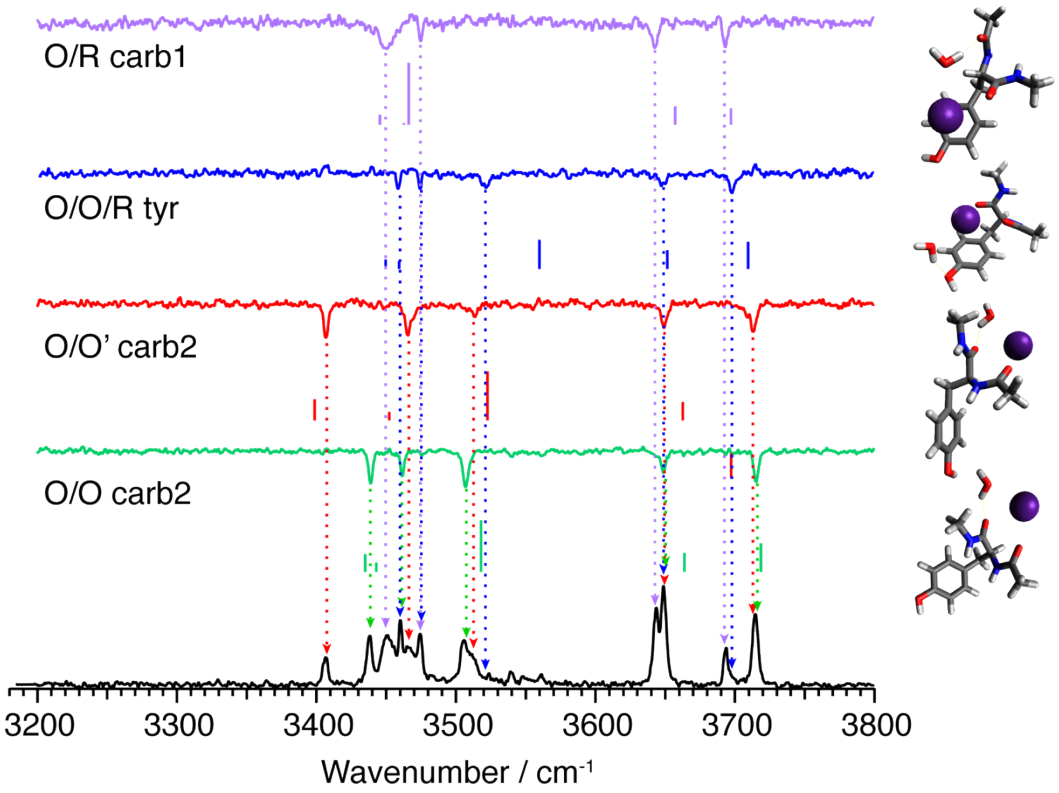

Fig. S 11 The IR-UV dip spectra of the hydrated Cs^+ complex with the 2-color IRPD spectrum at the bottom. The calculated spectrum and structure for each conformer are shown below/beside the experimental spectrum.

Table S 1 The assigned water binding site for each conformer

	O/O	**O/O'**	**O/O/R**	**O/R**
Li	Metal	Metal	Metal	N.D*.
Na	Metal	Metal	Tyr	N.D*.
Rb	Carb2	Carb2	Tyr	Carb1
Cs	Carb2	Carb2	Tyr	Carb1

* N.D. not detected

Theoretical spectra of the hydrated GYG-M$^+$ with different water binding sites

The theoretical spectra of each conformer, O/O, O/O', and O/O/R with the different water binding sites are shown below for each metal complex (Fig. S 12-Fig. S 20). The calculations were done at the M06-2X/cc-pVTZ, def2-TZVPP(M$^+$) level. The obtained harmonic vibrational frequencies were scaled by 0.945 for comparison with experimental spectra. The calculated spectrum in red was assigned to the observed experimental spectrum for the given conformer.

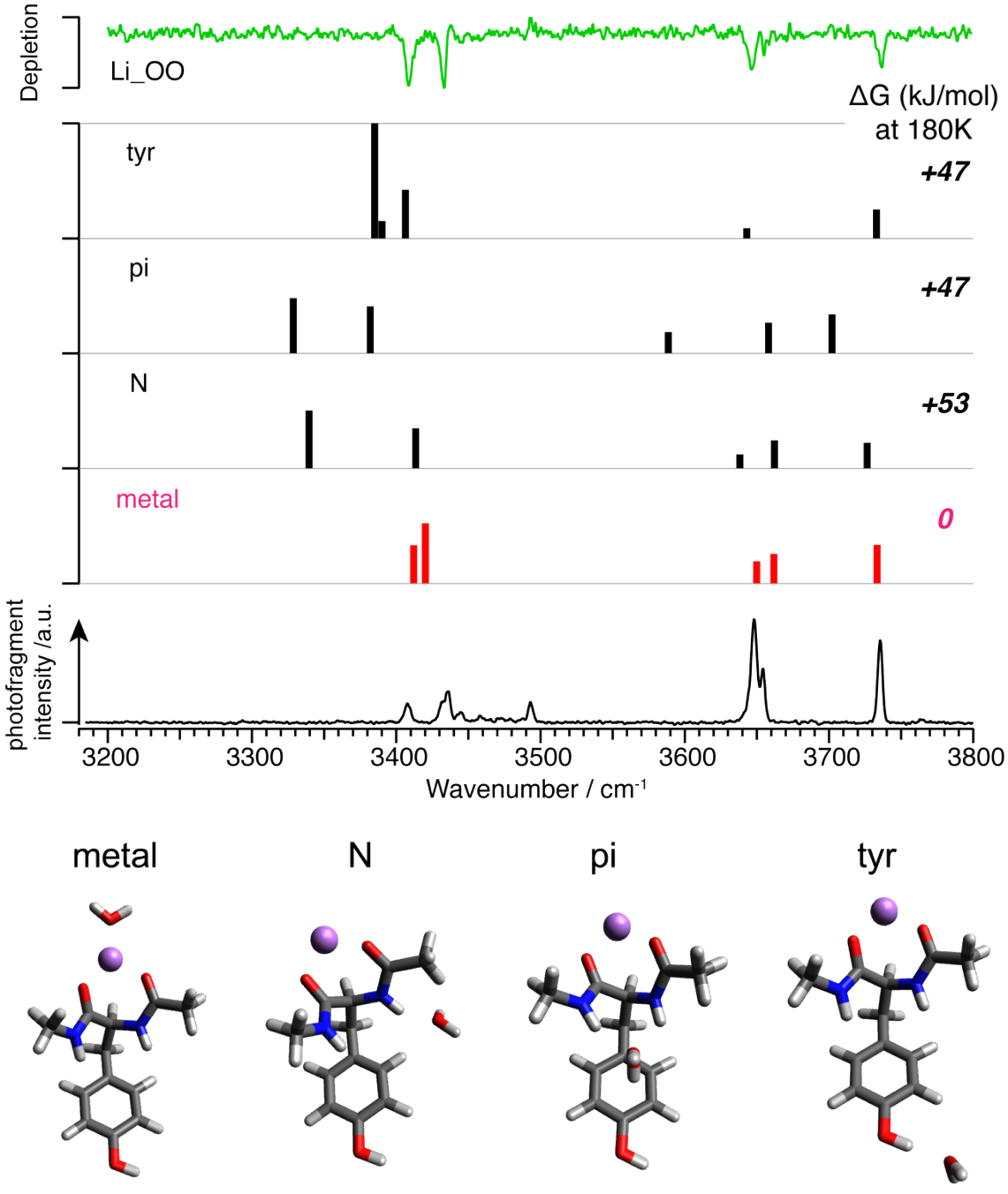

Fig. S 12 Theoretical spectra of O/O conformers of the hydrated Li complex with given water binding sites. The optimized structures are shown below.

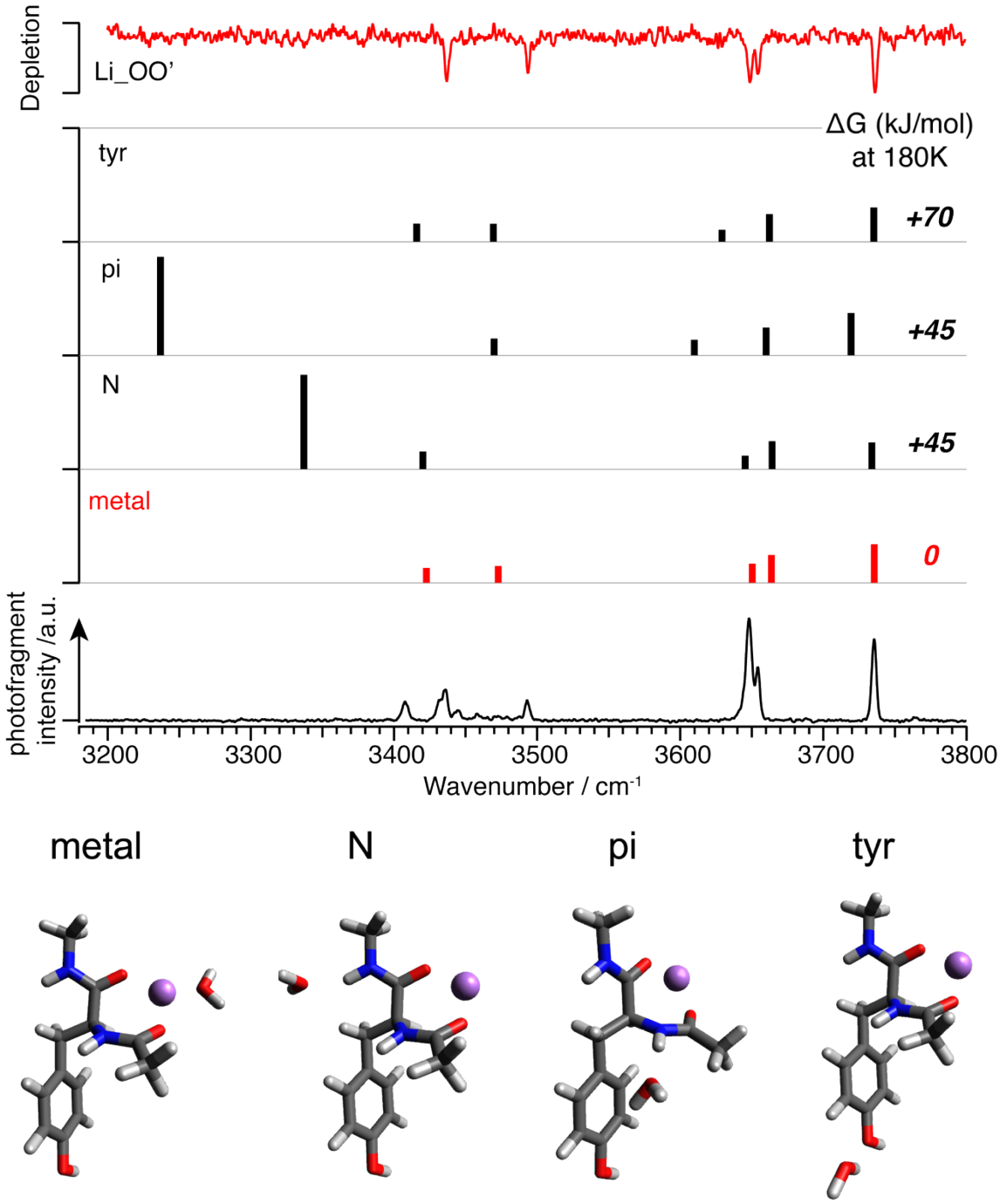

Fig. S 13 Theoretical spectra of O/O' conformers of the hydrated Li complex with given water binding sites. The optimized structures are shown below.

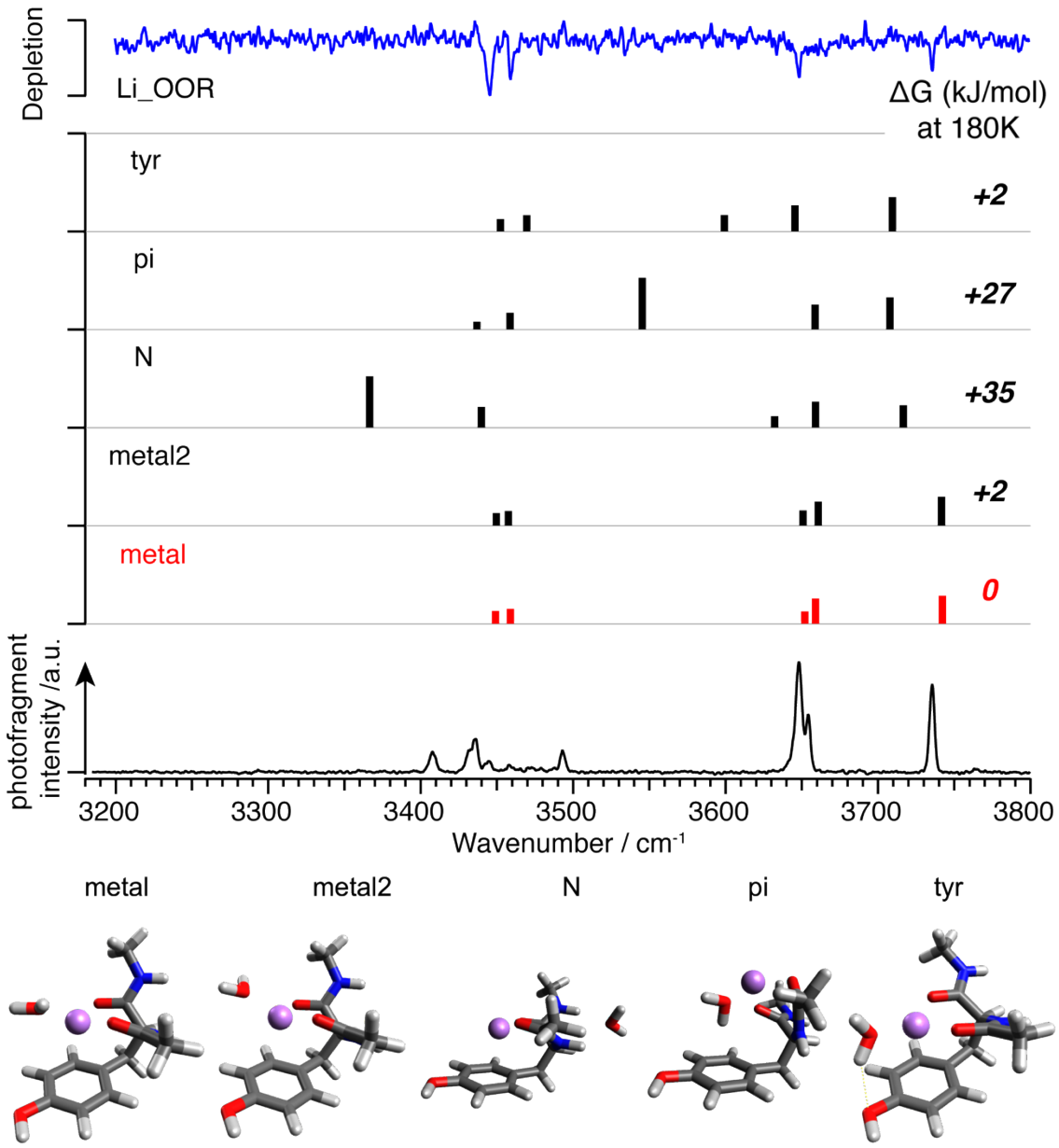

Fig. S 14 Theoretical spectra of O/O/R conformers of the hydrated Li complex with given water binding sites. The optimized structures are shown below.

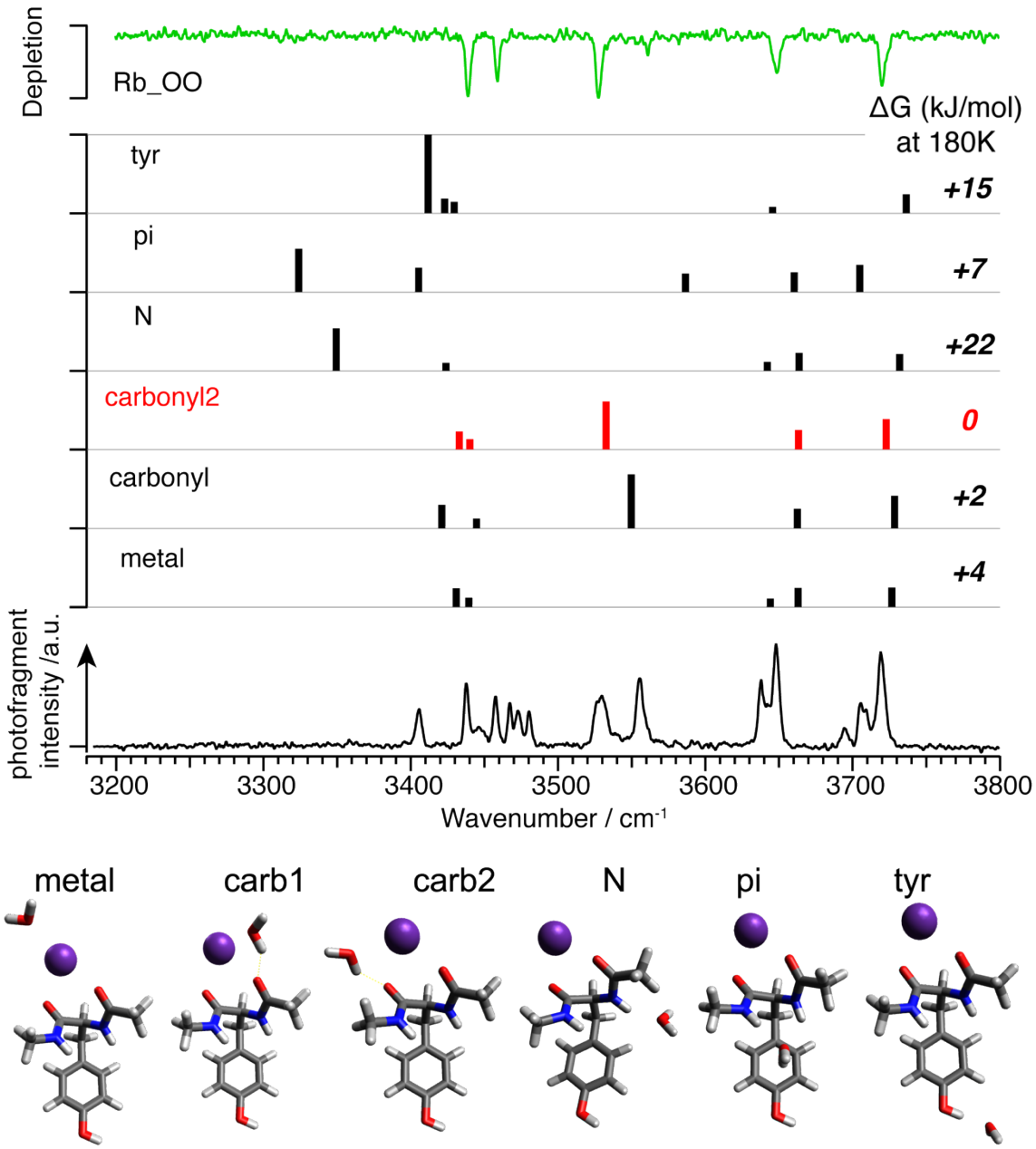

Fig. S 15 Theoretical spectra of O/O conformers of the hydrated Rb^+ complex with given water binding sites. The optimized structures are shown below.

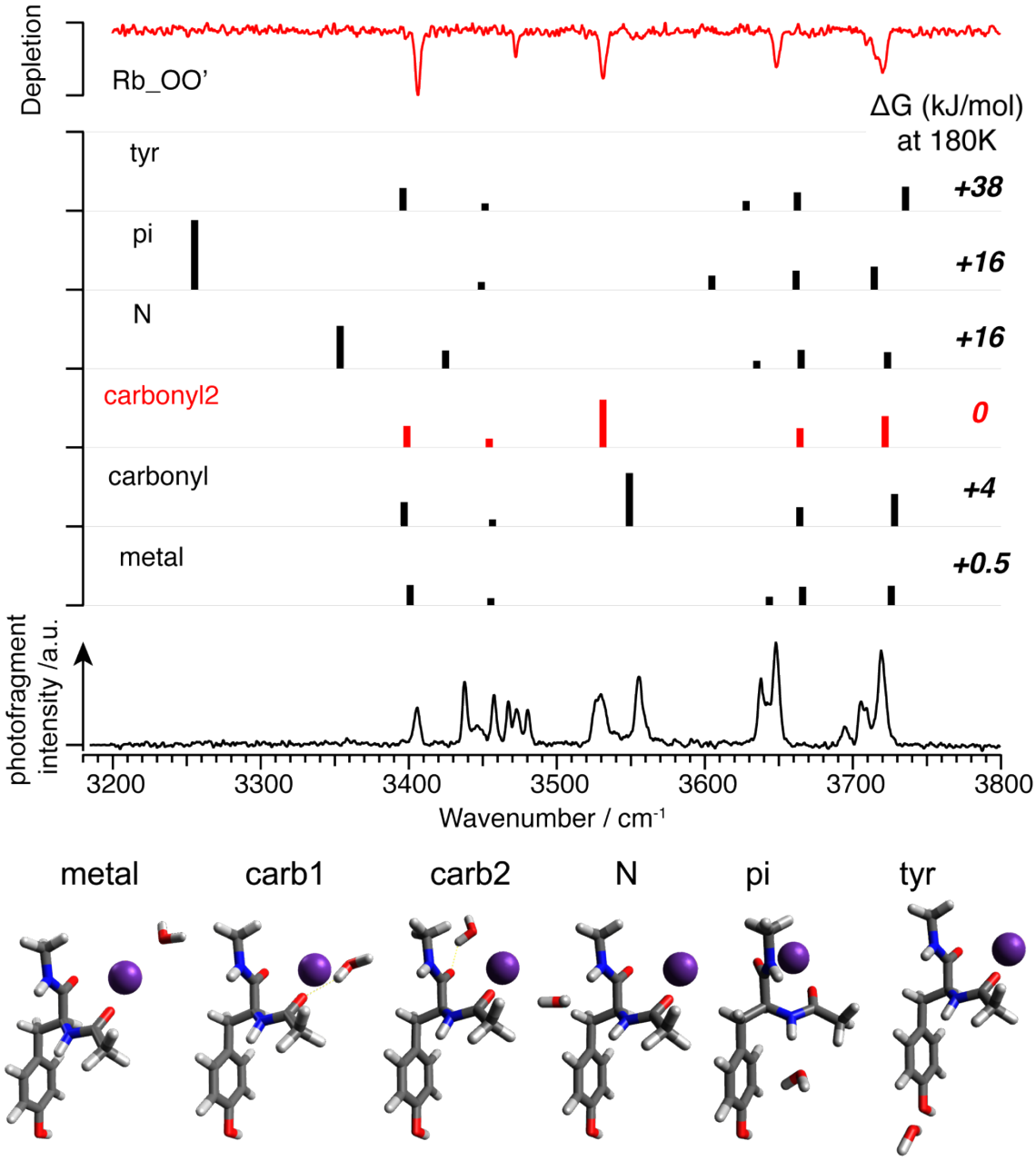

Fig. S 16 Theoretical spectra of O/O' conformers of the hydrated Rb^+ complex with given water binding sites. The optimized structures are shown below.

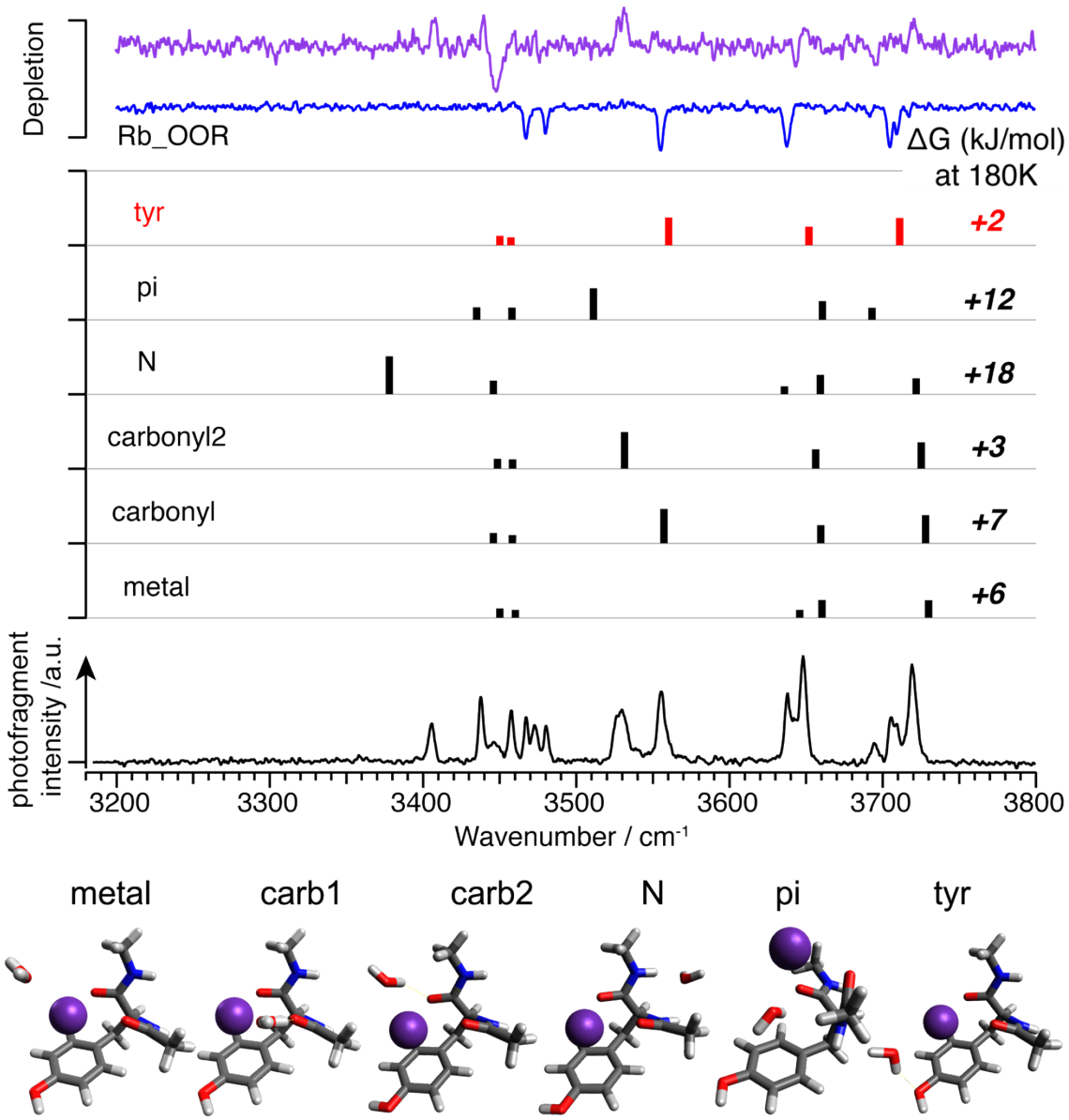

Fig. S 17 Theoretical spectra of O/O/R conformers of the hydrated Rb^+ complex with given water binding sites. The optimized structures are shown below.

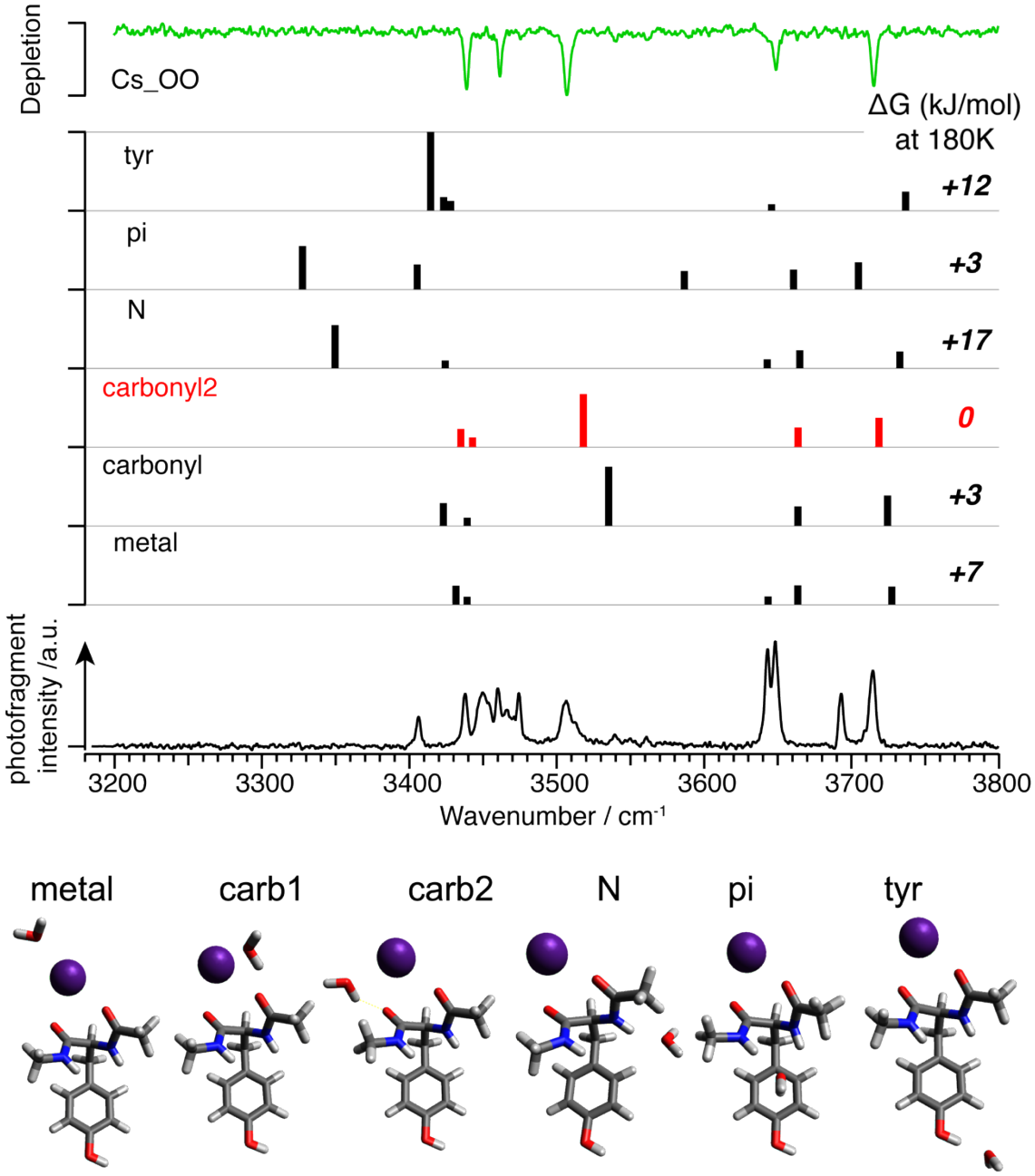

Fig. S 18 Theoretical spectra of O/O conformers of the hydrated Cs^+ complex with given water binding sites. The optimized structures are shown below.

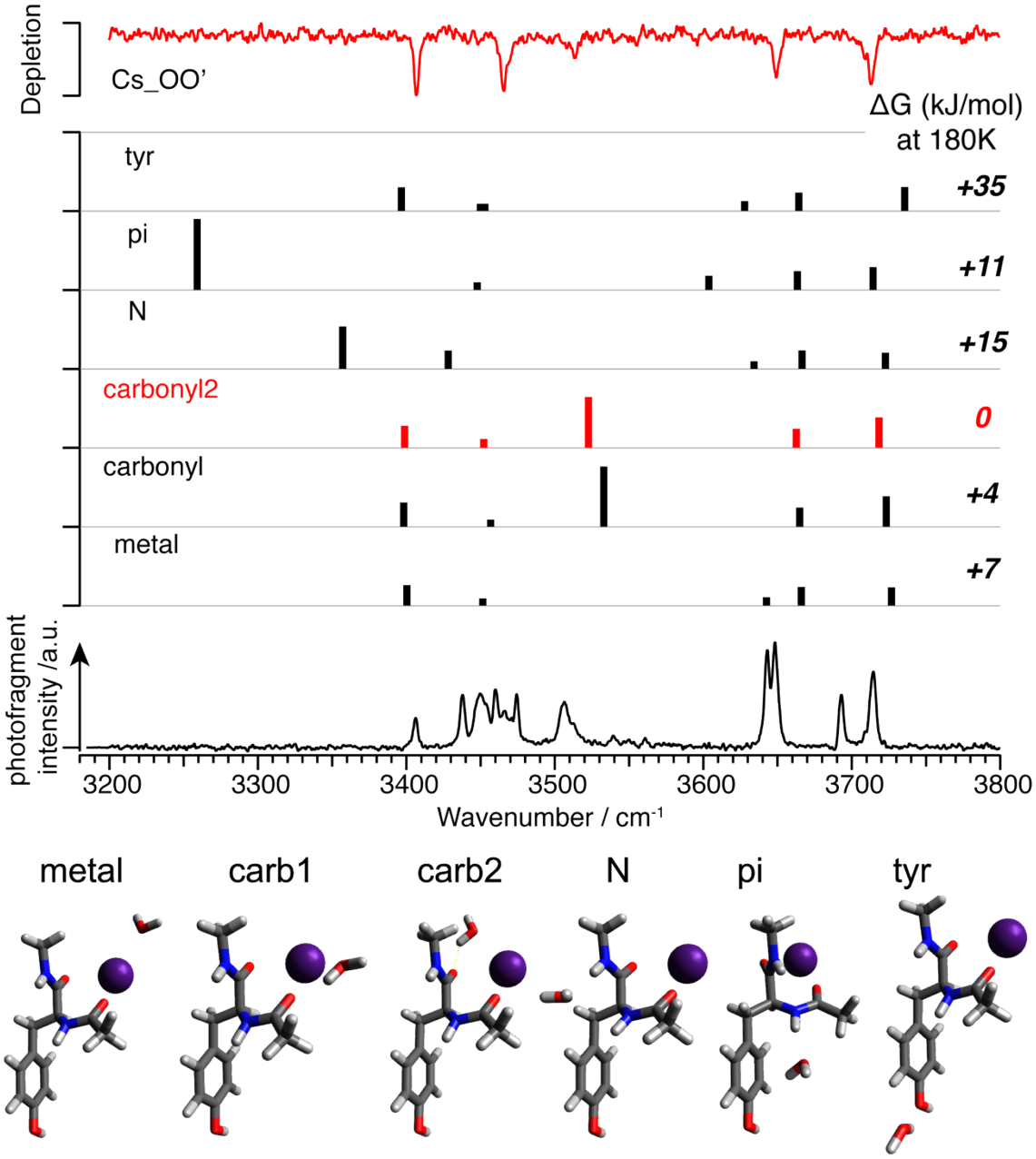

Fig. S 19 Theoretical spectra of O/O' conformers of the hydrated Cs^+ complex with given water binding sites. The optimized structures are shown below.

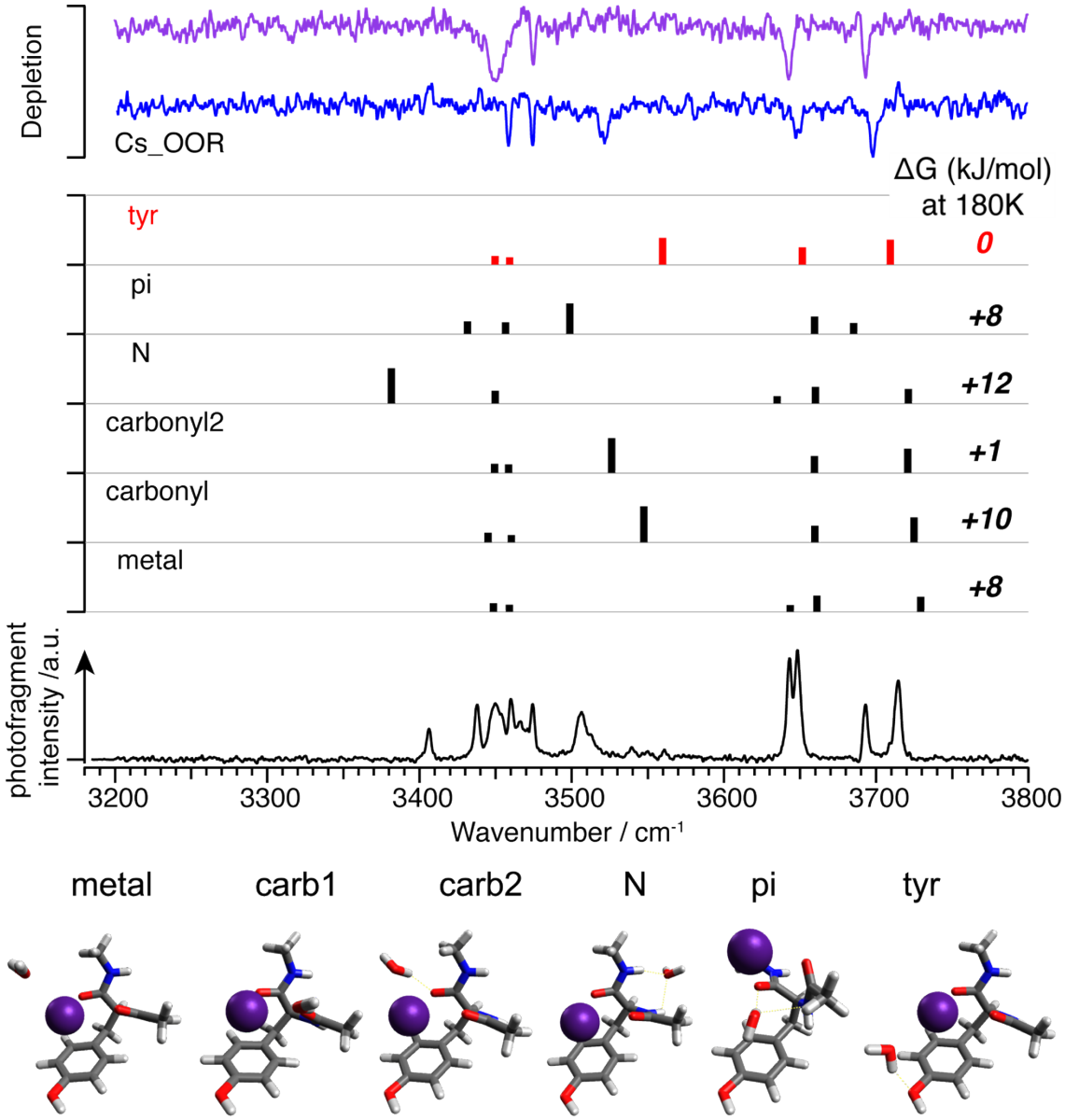

Fig. S 20 Theoretical spectra of O/O/R conformers of the hydrated Cs complex with given water binding sites. The optimized structures are shown below.

Peptide conformations

As discussed above, the fourth experimental spectra of the Rb^+ and Cs^+ complexes was inconsistent with any of the previously found peptide conformers. We carried out a further conformation search to seek out new structures that could reproduce the experimental spectra. Fig. S 21 a) shows the optimized structures, including the previously found O/O, O/O', and O/O/R conformers. Fig. S 21 b) represents the rotation axes that are important for peptide interconversion and the letters and the numbers above the arrows in Fig. S 21 a) show the rotation axes and the angles that connect the three conformers. The conformational analysis of the previously found conformers reveals that rotation around the Cα-Cβ axis (depicted as rotation "c" in Fig. S 21 b) of the O/O conformer (O/O1 in Fig. S 21 a) leads to the O/O' conformer (O/O' in Fig. S 21 a). Rotation around Cα-N and Cα-C axis in the O/O conformer (O/O1 in Fig. S 21 a) leads to the O/O/R conformer. Based on the relations of these conformers, the dihedral angles around the Cα-Cβ, Cα-N, and Cα-C axes (c, b, a in Fig. S 21 b, respectively) are expected to be most important for the peptide interconversion. To search for new conformers that can reproduce the experimental spectra for Rb^+ and Cs^+, we carried out a conformational search by rotating around these dihedral angles. In addition to the O/O' conformer, which is rotated 120 degrees around c, new conformers that are rotated by 120 degrees in the opposite way are found (O/O'2_1 and O/O'2_2). 180-degree rotation around this axis does not converge to a new structure. Additional 180 degree rotations about a and b in the O/O', O/O'2_1, and O/O'2_2 conformers converge to the O/O'1_{inv} and O/O'2_{inv} conformers as shown in Fig. S 21 a. For the hydrated species, the water molecule is attached to the carbonyl oxygens to make a hydrogen bond since the IR-UV dip spectra have significantly red-shifted OH stretches. In addition, the 180-degree-rotated initial structures around the c axis were also made since we expected that an additional hydrogen bond could stabilize these unstable non-hydrated structures. The theoretical spectra and optimized structures are presented in Fig. S 22 and Fig. S 23 respectively, for the Rb^+ complex. The relative free energies given in Fig. S 22 were determined at 180 K. The theoretical spectrum of O/O/R tyr in green is the conformer assigned to the third spectrum, which has similar NH stretch frequencies to the fourth one, but the H-bonded OH is not red-shifted as the experimental spectrum. The calculated spectra in blue come from the structure where the water is attached to the carbonyl oxygens of the newly found peptide conformers presented in Fig. S 21 and their structures are shown in Fig. S 22 a). Those in pink are the optimized structures (Fig. S 22 b)) that converged from the 180-degree-rotated initial structures around the c axis. From the calculated spectra, the O/O'1_{inv}_carb2(2) and O/R_carb1 show a relatively good agreement in the 3μ region. To confirm the assignment, the 6μ region was also measured for this Rb^+ and Cs^+ conformer. Based on the relative stability and the comparison in the 6μ region, the spectrum is assigned to the O/R_carb1 conformer. The calculated spectra of the Cs^+ complex are shown in Fig. S 24.

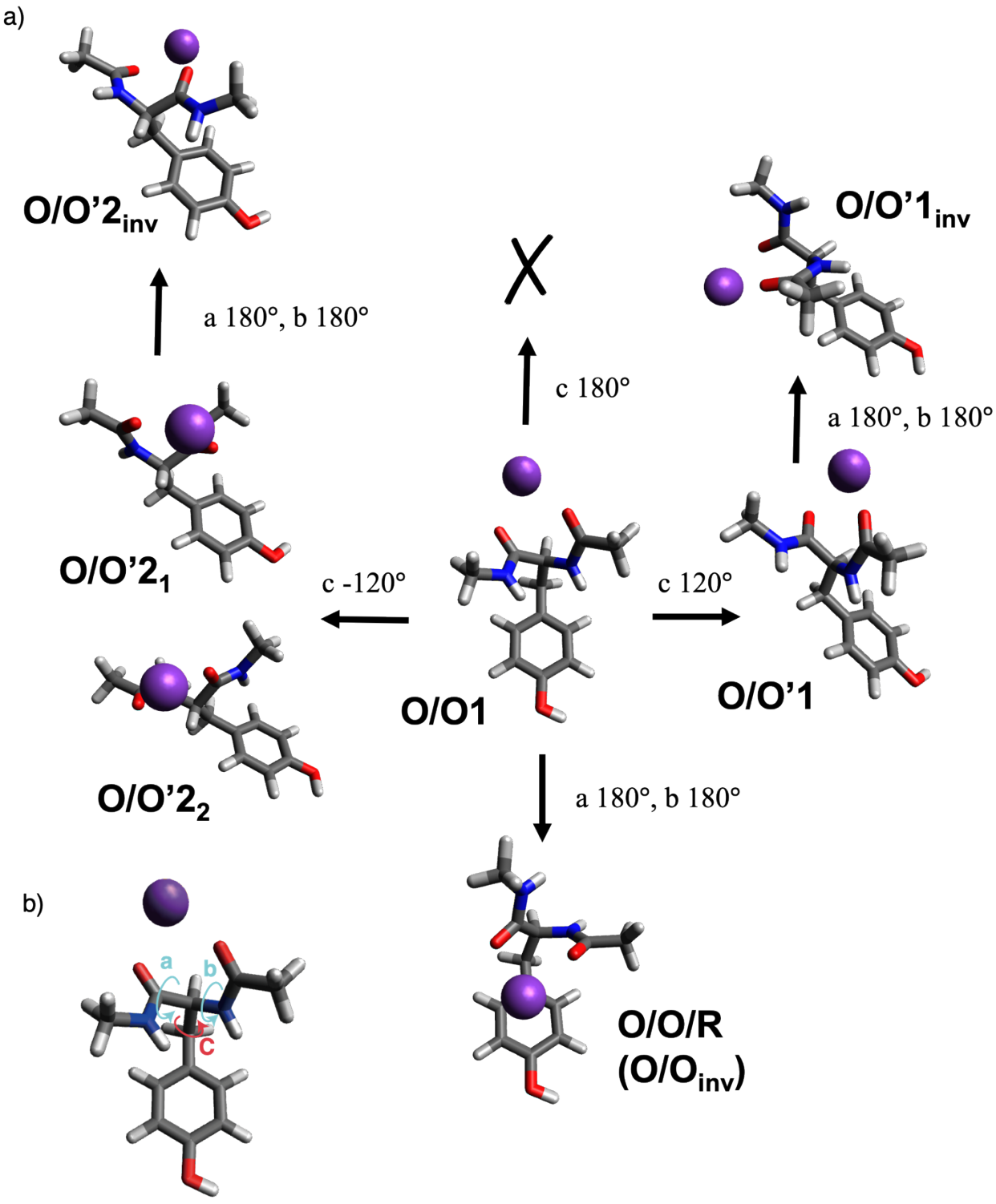

Fig. S 21 a) The optimized peptide conformations of non-hydrated GYG-M^+ and their relations. b) The dihedral angles that are relevant to the peptide interconversion.

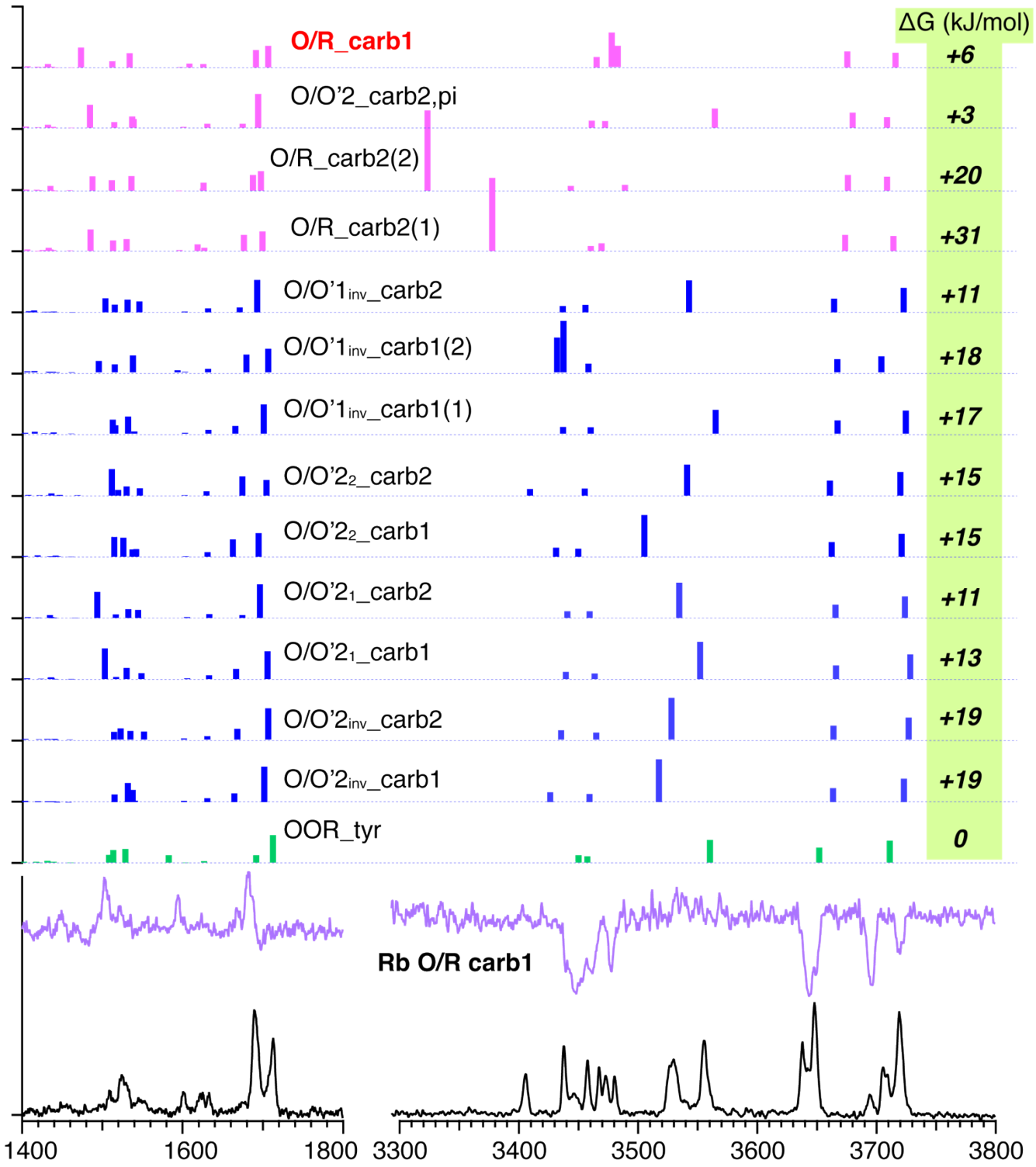

Fig. S 22 The theoretical spectra of newly found conformers for the Rb^+ complex.

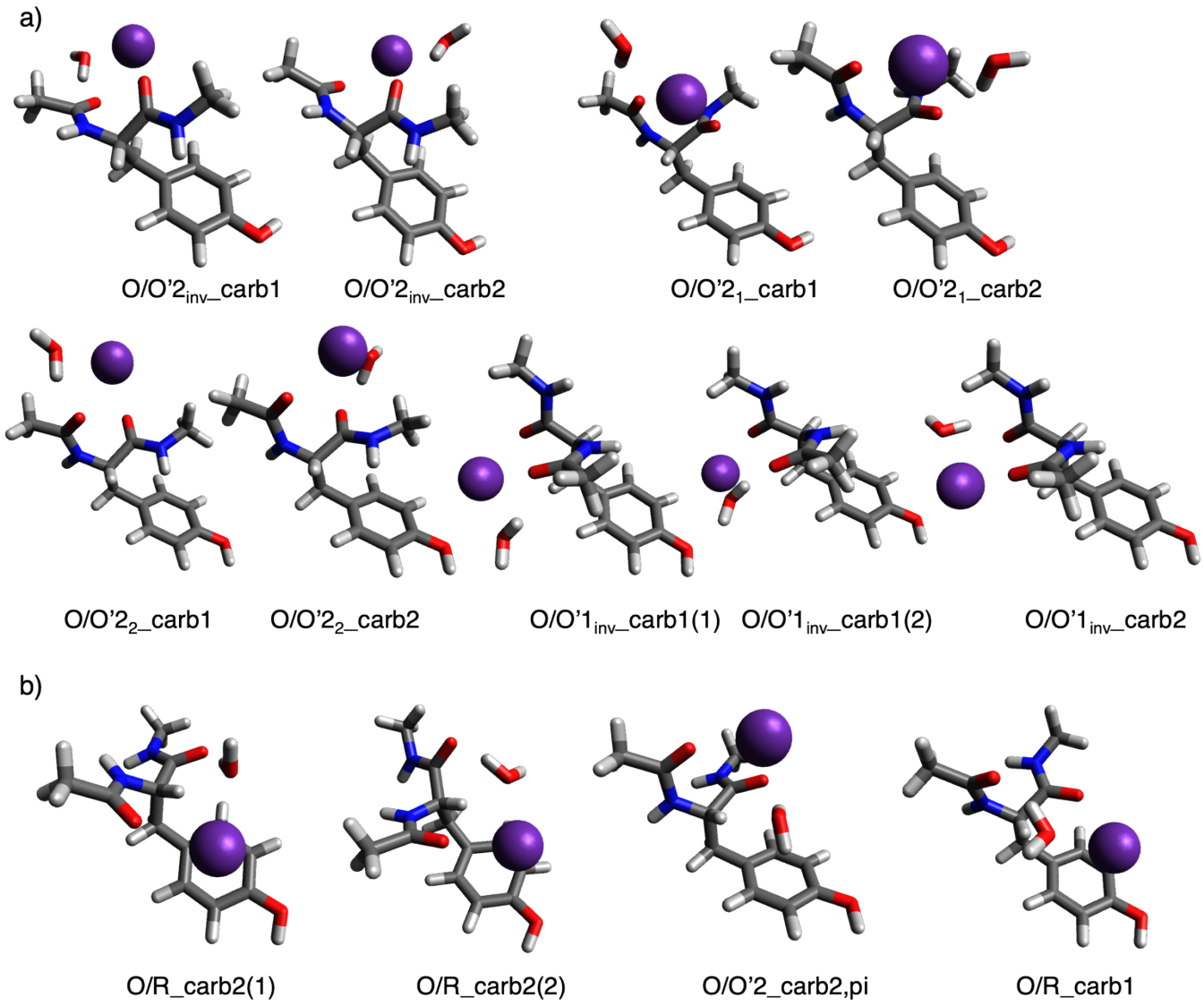

Fig. S 23 The optimized new conformers of Rb^+. a) Structures where water was attached to the conformers of non-hydrated species in Fig. S 21. b) Optimized structures whose initial structures are 180-degree-rotated from O/O around the c axis as shown in Fig. S 21.

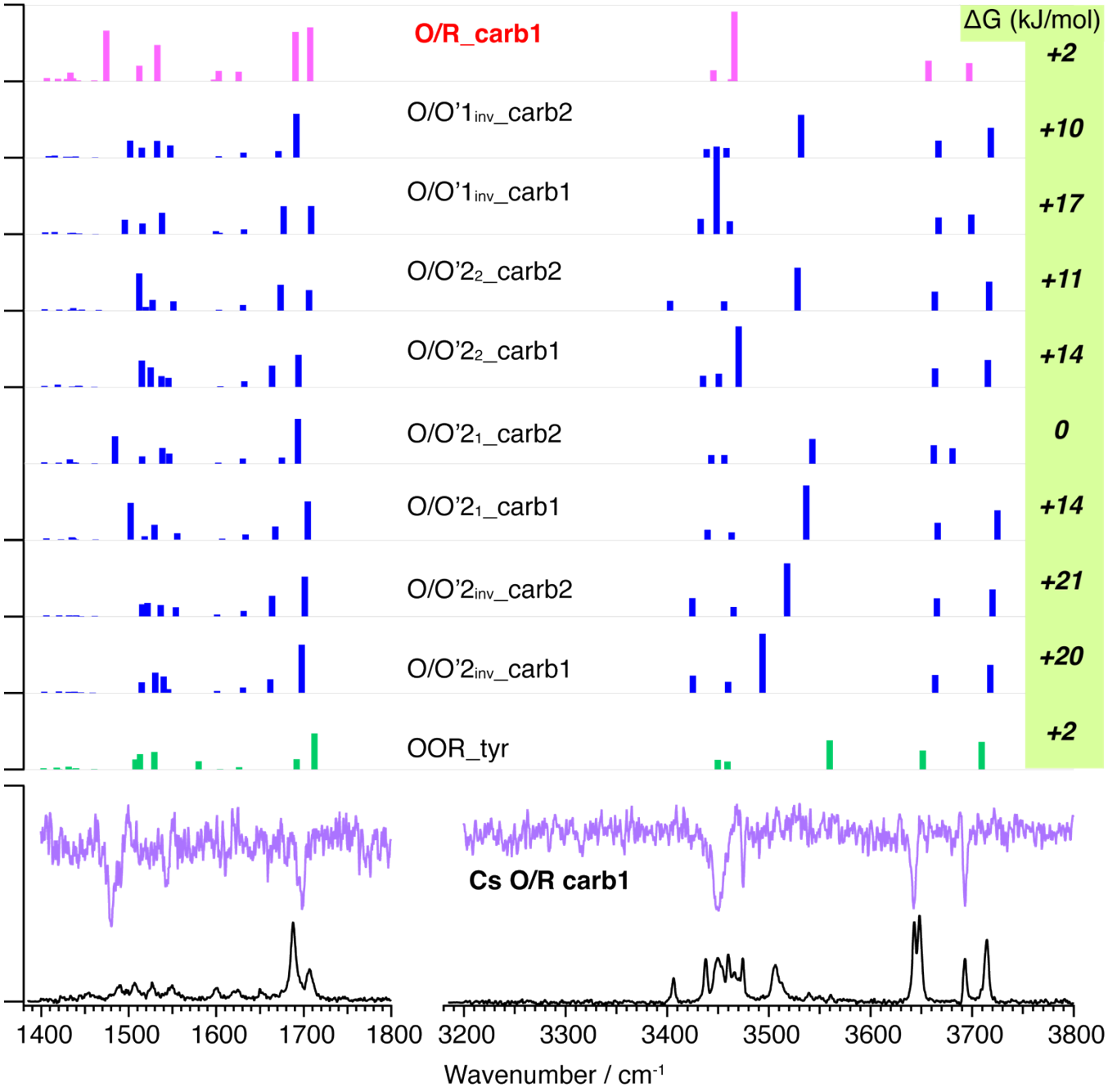

Fig. S 24 The theoretical spectra of newly found conformers for the Cs^+ complex.

UVPD spectra

The ultraviolet photodissociation spectra were measured in the same manner as the IRPD spectra. The UV fragments shown in Fig. S 26, generated by the irradiation from the UV laser, were monitored by a Time-of-Flight mass spectrometer as a function of the UV frequency. The frequency of the UV laser was fixed at one of the bands indicated by the arrows for the measurement of the IR-UV dip spectra.

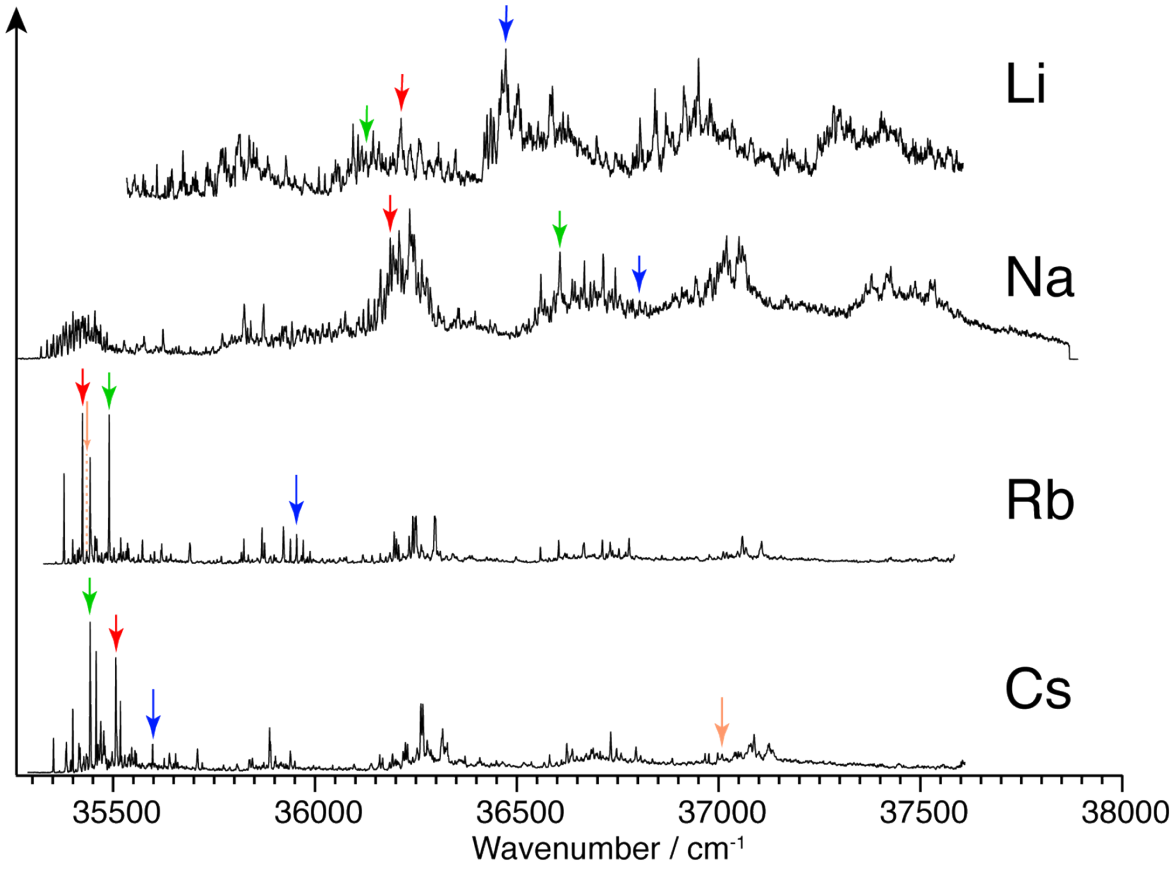

Fig. S 25 The UVPD spectra of the hydrated GYG-M^+ complexes. The arrows indicate the bands used for measuring IR-UV dip spectra for each conformer (green: O/O, red: O/O', blue: O/O/R, and orange: O/R)

UV fragments

The black and red spectra were measured without/with a UV laser. The presented IR-UV spectra were recorded by monitoring the relatively large fragment peaks at m/z=92, 136, 154 for Li^+ and 153 for Na^+. For the Rb^+ and Cs^+ complexes, the fragments were assigned to Rb^+ and Cs^+ ions, and these fragments were monitored for the IR-UV spectra. The conversion of the time of flight to m/z was carried out by specifying the m/z at the peaks of GYG-Li^+ -W and GYG-Li^+ generated by UV irradiation. For the Rb^+ and Cs^+ complexes, the m/z of the fragments was calculated from the time of flight and the m/z at the peaks of GYG-M^+-W and the time of flight of the fragments.

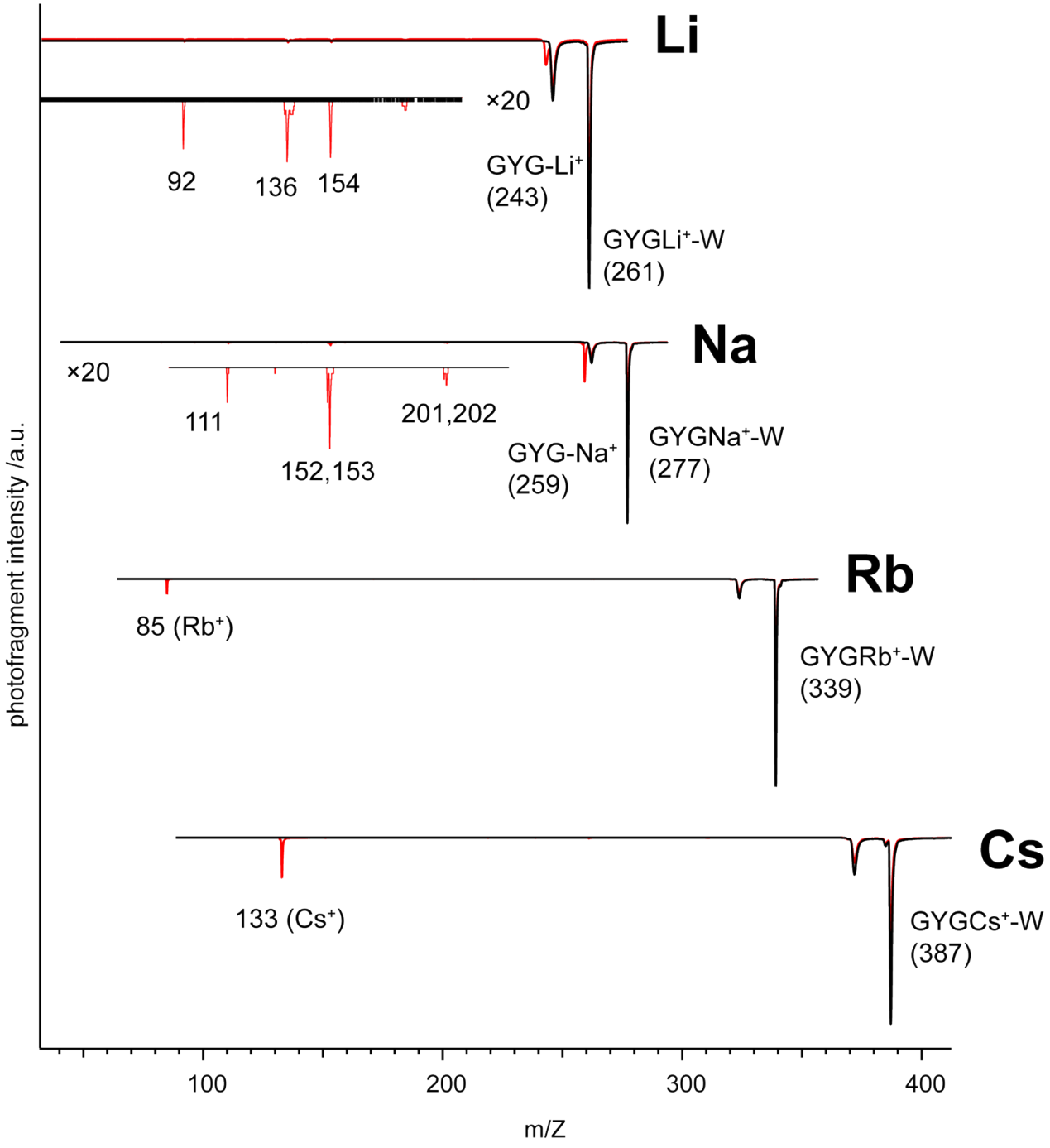

Fig. S 26 The ToF-MS spectra.

Functional dependence (H-bonded OH frequency)

The calculated H-bonded OH stretch was found to be sensitive to the functionals. Fig. S 27 display the theoretical spectra of the O/O conformer of the Cs^+ complex with water binding to the carbonyl oxygens. Each spectrum in red, blue, and green was calculated with B3LYP-D3, wB97XD, and M06-2X. The obtained harmonic vibrational frequencies are scaled by 0.956 for NH and free OH stretches, 0.962 for H-bonded OH stretches for B3LYP-D3, 0.942 for wB97XD, 0.945 for M06-2X. The H-bonded stretch calculated with B3LYP-D3 is relatively red-shifted compared to the spectra calculated with the other two functionals, even though the frequency obtained by B3LYP-D3 is scaled differently for this vibrational mode. The same trend was also observed for the K^+ and Rb^+ complexes.

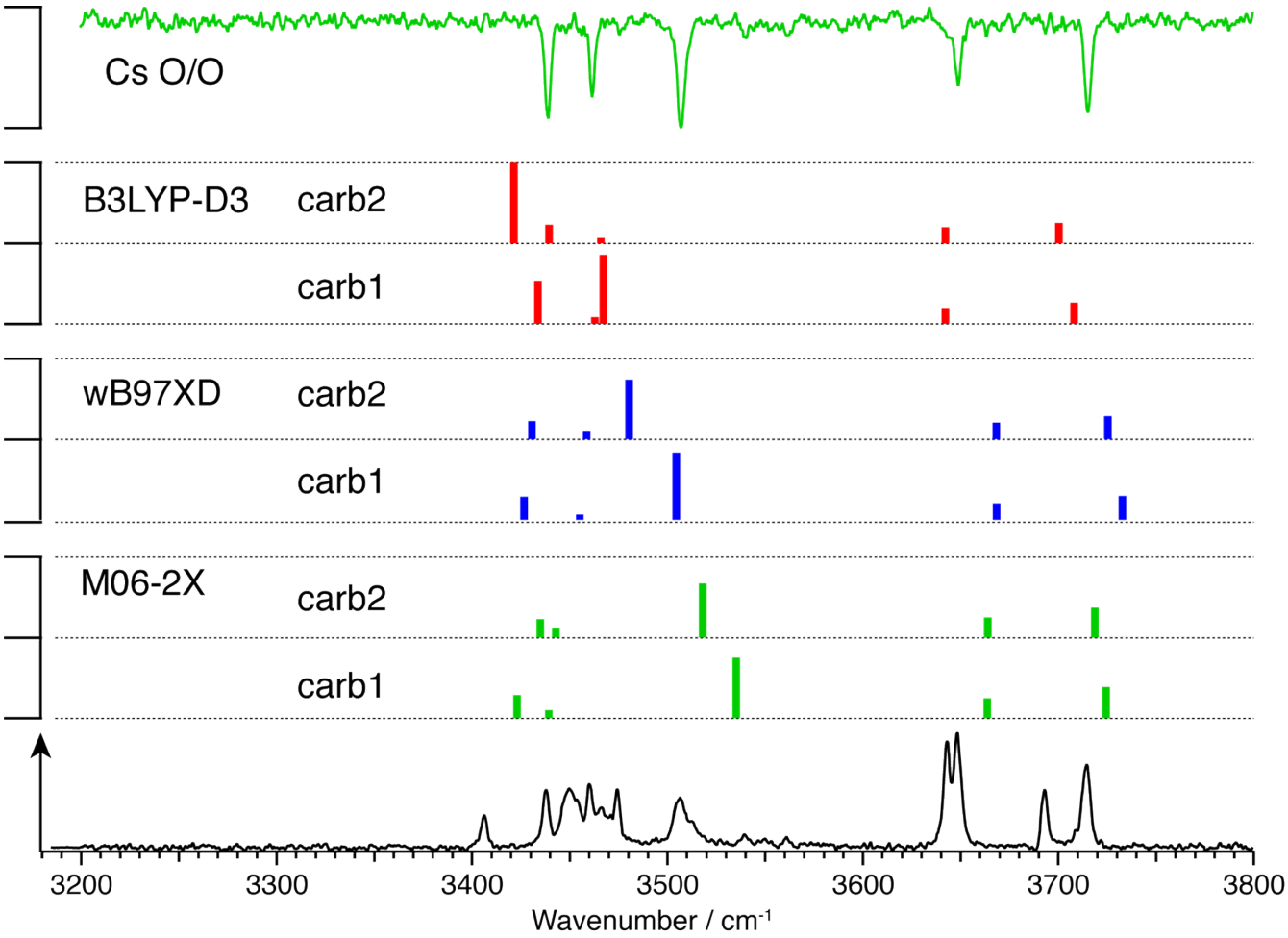

Fig. S 27 The functional dependence of the calculated IR spectra of the Cs O/O conformer.

Functional dependence (free energies)

The relative populations of the conformers for each hydrated GYG-M^+ are shown in Fig. S 28 for the three functionals: M06-2X, B3LYP-D3 and wB97DX. For each ion, at 300 K (close to physiological temperatures), there is considerable variation between each functional. As can be seen in Figures S 22 and S 24, the differences in the free energy for the various structures is often less than 20 kJ/mol. Given the complexity of the systems and the small differences in the energies, it does not come as a surprise that there is a lack of consistency between the three functionals. Unfortunately, this underscores the limitations of using computational results to predict with any degree of reliability the relative populations of the conformers, let alone attempting to predict, theoretically the temperature dependence.

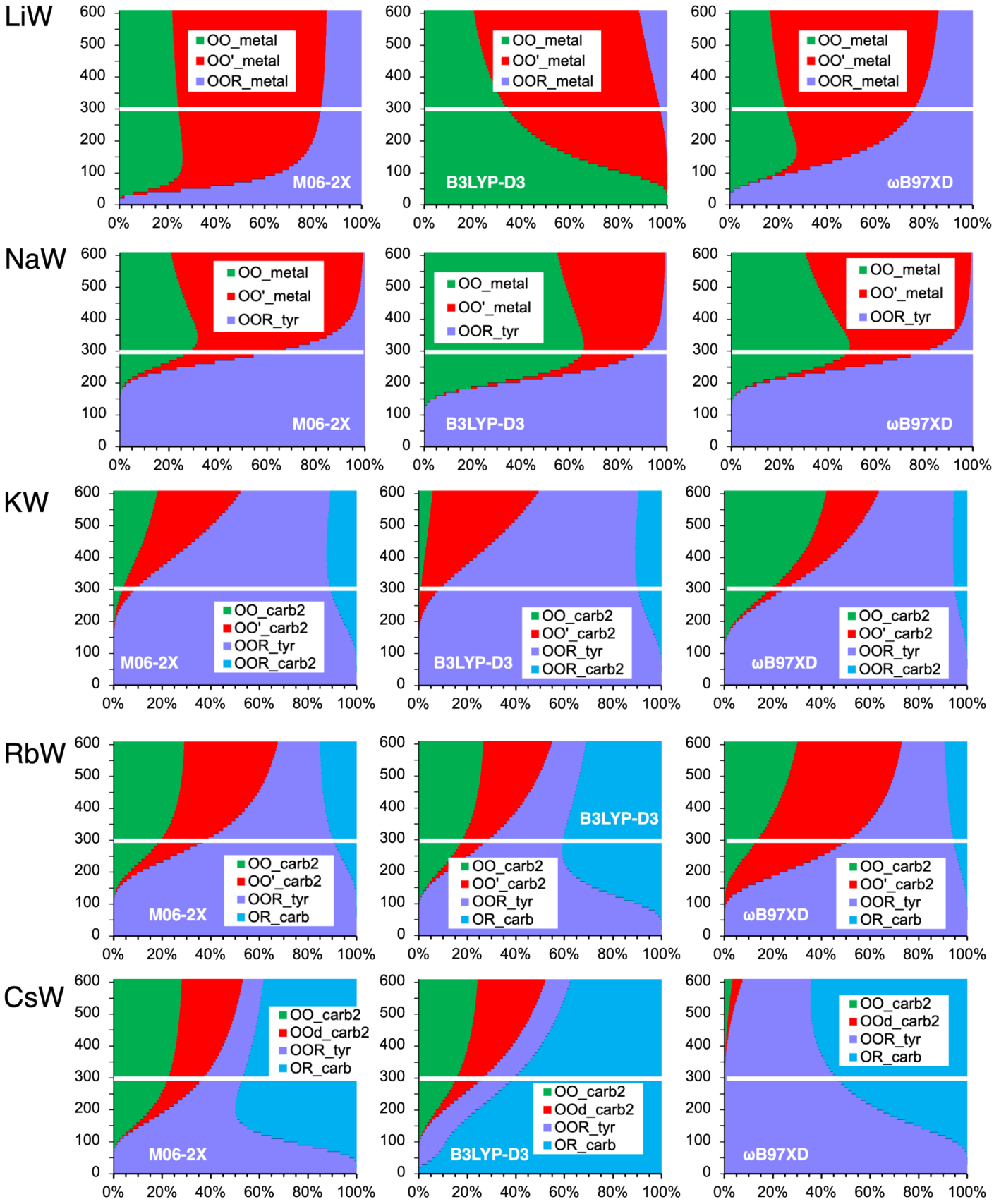

Fig. S 28 Functional dependence of the estimated conformational distributions of the hydrated GYG-M^+. The distributions were computed with three different functionals (M06-2X, B3LYP-D3, wB97XD) using the same basis sets (cc-pVTZ and def2-TZVPP for M^+).

Functional dependence (vibrational transition moment and population)

Table S 2 shows the conformer distributions estimated by using IR intensities calculated with three different functionals (M06-2X, B3LYP-D3, wB97XD). The functional dependence is quite small for most of the metal ions. The difference in Cs O/R is relatively large (64 %, 33%, 30 %, for M06-2X, B3LYP-D3, wB97XD respectively). As discussed in the main text, the population estimate of the Cs^+ complex was carried out by approximating the overlapping band of the O/R and O/O/R conformers are normalized only with the IR intensities of O/R because the contribution of O/O/R is small. The errors originating from this approximation are likely to be negligible compared to the functional dependence. Table S 3display the errors associated with the vibrational transition moments calculated using the three functionals. The standard deviations of the three different percentages calculated by using the three functionals for each conformer were calculated at each temperature and averaged for each conformer. The errors are relatively small except for the Cs^+ complex.

Table S 2 The conformer distributions at each temperature estimated by using the IR intensities of NH stretches that are calculated with the three functionals.

Metal	Temp	M06-2X			B3LYP-D3			wB97XD		
		O/O	O/O’	O/O/R+ O/R	O/O	O/O’	O/O/R+ O/R	O/O	O/O’	O/O/R+ O/R
Li	300	18	59	23	14	61	25	14	62	24
	270	19	60	21	15	62	23	15	63	22
	230	19	60	21	16	62	23	16	63	22
	180	18	60	21	14	62	24	15	63	22
	150	26	55	19	23	57	20	23	58	20
	130	26	55	19	22	57	20	23	58	20
	100	26	50	24	22	52	26	22	53	25
Na	300	46	42	12	51	25	25	37	50	13
	270	52	37	11	56	22	22	43	45	12
	230	54	36	10	58	22	20	45	44	11
	180	53	34	13	54	20	25	44	42	14
	150	50	34	16	51	19	30	42	41	17
	130	45	30	25	42	16	42	37	36	27
	100	55	34	12	58	20	22	46	41	13
K	270	57	32	11	63	25	12	57	31	11
	250	56	29	15	61	23	16	57	28	15
	230	56	28	15	62	22	16	57	27	15
	210	56	25	19	60	19	21	56	24	20
	180	49	23	29	52	17	30	49	22	29
	150	33	19	47	36	15	50	34	18	48
	130	38	24	38	41	18	41	38	22	39
	100	58	24	18	63	18	19	59	22	18
Rb	250	47	49	5	36	59	5	44	51	4
	230	47	48	5	36	58	6	44	51	5

	180	49	43	8	38	52	10	46	46	8
	150	45	36	18	35	44	21	43	39	18
	130	37	33	30	28	38	35	35	35	29
	100	48	46	6	37	56	7	45	49	6
	80	53	42	5	42	52	7	50	45	5
	230	23	14	64	39	28	33	42	28	30
	210	13	10	78	26	25	49	29	25	45
	180	14	10	76	28	24	48	32	25	44
Cs	150	11	6	82	25	18	57	29	18	53
	130	10	5	85	23	15	62	27	15	58
	100	10	5	85	24	15	61	28	16	57
	80	17	11	72	33	25	42	37	25	38

Table S 3 The averages of standard deviations of percentages of each conformer calculated at each temperature.

	O/O	**O/O'**	**O/O/R+O/R**
Li	~+/- 2%	~+/- 1%	~+/- 1%
Na	~+/-5%	~+/-10%	~+/-6%
K	~+/-2%	~+/-3%	~+/-1%
Rb	~+/-5%	~+/-4%	~+/-1%
Cs	~+/-8%	~+/-6%	~+/-14%

References

1. S. Ishiuchi, H. Wako, D. Kato and M. Fujii, *J. Mol. Struct.*, 2017, **332**, 45-51.
2. T. Negoro, K. Hirata, J. M. Lisy, S. I. Ishiuchi and M. Fujii, *Phys. Chem. Chem. Phys.*, 2021, **23**, 12045-12050.
3. R. Otsuka, K. Hirata, Y. Sasaki, J. M. Lisy, S. I. Ishiuchi and M. Fujii, *ChemPhysChem*, 2020, **21**, 712-724.
4. S. I. Ishiuchi, Y. Sasaki, J. M. Lisy and M. Fujii, *Phys. Chem. Chem. Phys.*, 2019, **21**, 561-571.